DIPLOMARBEIT

Titel der Diplomarbeit

Computing the Static Conductivity of Ionic Liquids

angestrebter akademischer Grad

Magister der Naturwissenschaften (Magister Rerum Naturalium)

Verfasser: Michael Haberler

Matrikel-Nummer: 0205555

Studienrichtung: A490

Betreuer: Prof. Othmar Steinhauser

Wien, am 14.03.2008

Danksagung

Ich möchte mich an dieser Stelle bei allen bedanken, die mich während meiner Diplomarbeit begleitet und unterstützt haben.

Mein Dank richtet sich insbesondere an meine Betreuer Prof. Othmar Steinhauser und Dr. Christian Schröder für die gute Zusammenarbeit und ihre fachliche Unterstützung, an meine Kollegen in der Arbeitsgruppe für ihre Hilfe im Arbeitsalltag und für das angenehme Arbeitsklima und natürlich an meine Familie, meine Freundin Bianca und meine Freunde in Wien und am Neusiedlersee, auf die ich immer zählen kann.

Zusammenfassung

In dieser Arbeit werden verschiedene Methoden erprobt, um die statische Leitfähigkeit ionischer Flüssigkeiten aus Molekulardynamik-Computersimulationen zu berechnen: die Green-Kubo, die Einstein-Helfand und die Nernst-Einstein Formel. Der springende Punkt dabei war einen Algorithmus für die Formeln zu finden, der einerseits große Mengen an Daten von Trajektorien miteinbezieht, um eine große statistische Stichprobe zu umfassen, und andererseits die Leitfähigkeit innerhalb eines vertretbaren Fehlers mit minimaler Rechenzeit zu ermitteln. Ähnliche Schwierigkeiten treten bei der Berechnung des Diffusionskoeffizienten auf, der in der Nernst-Einstein Formel proportional zur Leitfähigkeit ist. Der Diffusionskoeffizient, eine molekulare Größe, kann jedoch von einer kleineren statistischen Stichprobe bestimmt werden. Die untersuchten System ionischer Flüssigkeiten waren binäre Salze mit 1-butyl-3-methyl-imidazolium und 1-ethyl-3-methyl-imidazolium als Kationen, und Tetrafluoroborat, Hexafluorophosphat, Trifluoroacetat, Trifluoromethylsulfat, und Dicyanoimid als Anionen.

Abstract

The goal of this study is to determine the static conductivity of ionic liquids (IL) by molecular dynamics simulations using different approaches: The Green-Kubo formula, the Einstein-Helfand formula, and the Nernst-Einstein relation. Thereby expressions from statistical mechanics which involve position and velocity data from trajectories of systems of ILs are used. In practice the pivotal point proved to be the finding of an algorithm which on one hand analyzes large amounts of trajectory data for a high statistic accuracy and on the other hand yields the conductivity value within an acceptable error range with minimum computational effort. The calculation of the diffusion coefficient, a single particle property, which is the decisive factor of the Nernst-Einstein relation imposes the same constraints although with less need for high statistics. The IL systems under investigation were binary salts of 1-butyl-3-methyl-imidazolium and 1-ethyl-3-methyl-imidazolium as the cations, and tetrafluoroborate, hexafluorophosphate, trifluoric acid, trifluoromethylsulfate, and dicyanoimide as the anions.

Contents

I. INTRODUCTION

A. RTILs

Room temperature ionic liquids (RTIL), or shorter ionic liquids (IL), define a class of salts which remain liquid at ambient temperature, as opposed to commonly known salts, such as the rock salt NaCl which starts to melt at 801°Celsius.

Known since the beginning of the 20th century, ionic liquids have only attracted major research interest in the past three decades when compounds of this class with tractable physical properties and feasible application possibilities were first synthesized. The novel features of these ionic liquids were largely due to their organic constituents with anisotropic shape and diffuse charge distribution. Today's most intensively studied ionic liquids consist mainly of substituted imidazoliums, pyridiniums, and pyrrolidiniums, tetraalkyl ammoniums, and phosphoniums as cations and organic, as well as anorganic, anions, like halides and pseudohalides, borates, phosphates, alkyl sulfates, and sulfonates, triflates, and trifluoroacetates.

Introducing functional groups and combining different anions and cations opens a vast regime of possible ionic liquids with correspondingly differing physical properties. Some estimate the number of accessible ionic liquids as high as a trillion[1] (10^{18}). They all reveal negligible vapor pressure which is due to their ionic nature and are therefore non-volatile. The newest versions of ILs also show up other desireable physical properties, at least to a certain extent, such as non-corrosivity, air- and water-stability, high thermal, chemical and electrochemical stability and they readily dissolve hydrophobic and hydrophilic substances. Choosing an ionic liquid with appropriate characteristics for a given problem has led to the charming neologism "Task-Specific Ionic Liquid".

Summing up, ionic liquids can prove as an attractive, environmentally benign replacement for volatile organic solvents in synthesis and catalysis (e.g. reaction medium, catalysator), biotechnology (e.g. dissolution of cellulose), process engineering (e.g. desulfurization of oil), analytical chemistry (e.g. capillary coating, eluent additive) and electrochemistry (e.g. conductant in batteries), to name a few.

B. Computational and Experimental Investigation of RTILs

To predict the physical properties of the plethora of possible ionic liquids without ever going into the trouble of synthesizing them, computer simulation of these materials - among chemical intuition and extrapolation from known compounds - is the method of choice. It is an excellent way to gain a deeper understanding how atomic-scale characteristics of a system (i.e. the behavior of electrons and nuclei of molecules) determine macroscopic properties (thermodynamic properties: density, crystal structure, melting point, heat capacity, enthalpy, free energy, gas solubility, water miscibility and transport properties: self-diffusivity, viscosity, electrical and thermal conductivity). In contrast, only a few experimental methods allow a comparably detailed examination.

Since we are dealing with mobile charged molecules electrical conductivity emerges as topic of increased interest. Additionally, the anisotropic shape of ILs induces electric polarity which in turn brings about electric permittivity, measurable as the dielectric constant. For the experimentalist, these two phenomena, conductivity and dielectric response, combine to an effect described by the term of the **Frequency Dependent Generalized Dielectric Constant** $\Sigma(\omega)$. Specially designed implementations of dielectric spectrometers can record the corresponding spectrum of ILs[2,3].

Starting from first principles of molecular geometry and interaction computer simulation, to be precise molecular dynamics simulation, enables as well the calculation of a dielectric spectrum, i.e. $\Sigma(\omega)$. Thus one can compare experimental and simulated data and thereby validate the model of molecular interaction, the force field. Clearly, it is possible to comprehend the different contributions of molecular motion, i.e. translation, rotation and vibration, to both the frequency dependent conductivity $\sigma(\omega)$ and dielectric constant[4] $\epsilon(\omega)$.

In this work I focus on the **Static Conductivity** as part of the dielectric spectrum of several ionic liquids. It can be computed from molecular dynamics simulation data, the trajectory, on the basis of statistical physics in two ways, the Green-Kubo and the Einstein-Helfand formula. The Nernst-Einstein relation provides an approximate link between conductivity and the **Diffusion Coefficient** which itself can be calculated from trajectory data using analogous Green-Kubo and Einstein expressions. The derivation for these formulas will be explained in the Theory section and their actual implementation in programs will be presented in the Methods section. Finally, the outcome of the calculations and a critical

analysis and interpretation are given in the Results and Discussion Section.

It has to be added, that, experimentally, the static conductivity is not measured by dielectric spectroscopy but by a direct current method. The diffusion constant can be determined experimentally in various ways, like pulsed-field-gradient spin-echo NMR, or neutron-diffraction.

II. THEORY

A. Molecular Dynamics Simulation

With the concept of classical molecular dynamics, it is possible to simulate atomic motion of reasonably sized systems (up to hundred thousands of atoms) and time periods (up to tens of nanoseconds) on commodity computers and computer-clusters.

At the heart of molecular dynamics lies the Born-Oppenheimer approximation which is a prerequisite to separate nuclear and electronic motion. In this regard, the interaction function, or potential, is constituted by the electrons. The potential ($U(\mathbf{r}_1, ..., \mathbf{r}_N)$) in turn is modeled by an ansatz using empirical terms, known under the acronym force field, consisting of terms for atom bonds, angles between two bonds, dihedral angles, and for non-bonding interactions[5,6]. The resulting (Newtonian) equations of motion for the nuclei (particles), with m_i the mass of the ith nucleus, are (Bold-lettered variables denote vectors, e.g. $\mathbf{r} := \vec{r}$.):

$$m_i \frac{\mathrm{d}^2 \mathbf{r}_i}{\mathrm{d}t^2} = \nabla U(\mathbf{r}_1, ..., \mathbf{r}_N) \qquad i = 1, ..., N \qquad \text{for a N-particle system} \qquad (1)$$

Numerical integration returns positions ($\mathbf{r}_i(t)$) and velocities ($\mathbf{v}_i(t)$) for the individual atoms which make up a trajectory, a "curve" in 6N-dimensional space, the phase space, as a function of time. The 6N stems from 3N dimesions for the positions and another 3N for the velocities, or momenta, of N particles. If there are no external forces, the system is in equilibrium.

There remain a couple of issues in computer simulation, like the long-range electrostatic potential, the center-of-mass and energy drift due to numerical integration, temperature fluctuations, to name a few, which can be dealt with in different ways which are treated in the monographs 5, 7, and more sophisticated in Ref. 6. The concepts of statistical mechanics enable to interpret and analyze these trajectories in a way that relevant physical values can be computed, e.g. the static conductivity in our case. These theories often include statements, such as average over the time from zero to infinity, or over all points in phase space (almost $(6N)!$), which is impossible to achieve on the computer. Fortunately, for a given accuracy an averaging over a reduced sample is often sufficient. The afore-mentioned "reasonably sized systems and time periods" thus refer to limited available trajectory data which nevertheless satisfyingly reproduce expected results.

In the subsequent sections emphasis is put on the investigation of the static conductivity of ILs by molecular dynamics simulations which is based as well on a complex theoretical framework and requires special care upon calculation from trajectory data.

B. Static Conductivity

If an electrical field $\mathbf{E}_0$, where $\mathbf{E}_0$ stands for the Maxwell-field, is applied to a conducting system an electrical current $\mathbf{j}$ can be observed. The relation between the current and a given field is described by the empirical finding, **Ohm's Law**

$$\mathbf{j} = \sigma \cdot \mathbf{E}_0 \tag{2}$$

where σ stands for the conductivity of the system. Thus, in experiments it is necessary to apply an electrical field to the system to measure its conductivity which brings about non-equilibrium conditions. Unfortunately, in computer simulations it is inconvenient to include an external field into the equations of motions, e.g.

$$m_i \frac{\mathrm{d}^2 \mathbf{r}_i}{\mathrm{d}t^2} = \nabla U(\mathbf{r}_1, ..., \mathbf{r}_N) + \sum_i q_i \mathbf{E}(t) \tag{3}$$

(with q_i the charge of the ith particle) because it would either lead to a rise in temperature, a drift in energy and center-of-mass, or it would provoke currents outside the linear response regime[8] if the field was too strong, or it would be swamped by noise if it was too weak. Despite these difficulties also non-equilibrium computer simulations are established[9].

However, the **Fluctuation-Dissipation Theorem** states that small fluctuations, in other words the noise, of dynamical variables in equilibrium systems behave, or literally relax, in just the same way as the dynamic variable in a non-equilibrium system induced by an external field would. The mathematical explanation and proof has been brought about by R. Kubo in 1957 for **Transport Processes**[10], the conjugate fluxes to mechanical fields. The **Green-Kubo Formula** for conductivity is

$$\mathbf{j} = \frac{\langle \Delta \mathbf{J}(\omega) \rangle}{V} = \underbrace{\left(\frac{1}{V k_B T} \int_0^\infty e^{i\omega t} \langle \mathbf{J}(t) \mathbf{J}(0) \rangle \, \mathrm{d}t \right)}_{=\sigma(\omega)} \mathbf{E}(\omega) \tag{4}$$

16

with $\mathbf{J}$ being the current, V the volume of the system, k_B the Boltzmann constant, T the temperature, and $\langle \cdots \rangle$ marking the time or ensemble average. For this reason it is perfectly possible to simulate equilibrium systems, record the occurring fluctuations in dynamical variables, in this case the current, and calculate non-equilibrium properties, the conductivity. This property which is the proportionality factor that relates the current to its field is called more generally the **Transport Coefficient**.

Another pertinent transport process is **Diffusion** with the diffusion constant D as transport coefficient which is expressed according to the Green-Kubo Formula as

$$D = \frac{1}{3} \int_0^t \langle \mathbf{v}_i(t) \mathbf{v}_i(0) \rangle \, \mathrm{d}t \tag{5}$$

with $\mathbf{v}_i$ being the velocity of the ith particle. The **Nernst-Einstein relation** connects the two transport coefficients under the condition that electrolyte interaction is negligible

$$\sigma = \frac{1}{V k_B T} \left(z_+^2 e^2 n_+ D_+ + z_- e^2 n_- D_- \right) \tag{6}$$

Here, e stands for the electron charge, z for the net charge on the ion, and n for the total number of ions from one species. Because in ILs the electrolytes interact strongly this relation overestimates the conductivity by roughly two thirds. The decisive part missing in the Nernst-Einstein relation are the cross-correlations of the single particle velocities, i.e. $\langle \mathbf{v}_i(t) \mathbf{v}_j(0) \rangle$ for $i \neq j$ of which above all the cation-anion cross-correlations would significantly decrease the value of the conductivity.

Kubo also pointed out the equivalence of his formula of the diffusion coefficient to the **Einstein Formula of Diffusion** (equation (62)) derived from the theory of Brownian motion, i.e. from statistical arguments (random walk). Picking up this line of reasoning E. Helfand devised an analogous relation between the mean square displacement of the translational dipole moment, the integral of the current $\mathbf{M}_J = \int_0^\infty \mathbf{J} \mathrm{d}t$, and the conductivity

$$\sigma(\omega = 0) = \frac{1}{3 V k_B T} \int_0^\infty \langle \mathbf{J}(t) \mathbf{J}(0) \rangle \, \mathrm{d}t \tag{7}$$

$$= \frac{1}{6 V k_B T} \lim_{t \to \infty} \frac{\langle \Delta \mathbf{M}_J(t)^2 \rangle}{t} \tag{8}$$

17

In the next section the theoretical rationale behind the listed expressions for the conductivity is given.

C. Derivation of the used Formulas

To justify the calculation of conductivity from trajectory data the formulas used will be derived in this section.

1. Green-Kubo Formula

In short, the Green-Kubo equation relates linear transport coefficients to the time-dependence of equilibrium fluctuations in the conjugate flux of a system to an external field. It can be derived in various ways, using the Langevin-equation (non-Markovian random forces), the fluctuation-dissipation theorem (spontaneous entropy production), or statistical mechanics (perturbation theory).

Here, I will take the latter approach and start out from advanced concepts of classical and statistical mechanics to rationalize the **Linear Response Theory** (For an introduction to these see Ref. 11 and 9.). With the definition of correlation functions it is then straightforward to understand the Green-Kubo Formula[10,4].

In our case, we observe equilibrium fluctuations of the total current $\mathbf{J}$, the conjugate flux to an external electric field $\mathbf{E}$, and link them to the transport coefficient, the static conductivity σ.

$$\mathbf{J}(\mathbf{v}_i(t)) = \sum_{i=1}^{N} q_i \mathbf{v}_i(t) \qquad \mathbf{v}_i(t) = \frac{\mathrm{d}\mathbf{r}_i(t)}{\mathrm{d}t} \tag{9}$$

Considering an N-particle system and using the ansatz of **Perturbation Theory**, we can split up the Hamilton-function of the system ($\mathcal{H} := \mathcal{H}(\mathbf{r}_i, \mathbf{p}_i, t) \quad i = 1, ..., N$) into an unperturbed part $\mathcal{H}_0$ and the perturbation part $\mathcal{H}'(t)$:

$$\mathcal{H} = \mathcal{H}_0 + \mathcal{H}'(t) \tag{10}$$

For simplification we assume the external field $\mathbf{E}$ to be homogeneous and equal to the Maxwell-field $\mathbf{E}_0$. The perturbation part $\mathcal{H}'(t)$ can then be expressed as a product of a

perturbing field, in our case the electric field $\mathbf{E}(t)$, and its coupling variable, the collective dipole moment $\mathbf{M}_{tot}$:

$$\mathcal{H} = \int_V \rho(\mathbf{r})U(\mathbf{r})\,d\mathbf{r} = -\int_V \rho(\mathbf{r})\mathbf{r}\mathbf{E}\,d\mathbf{r}$$

$$= -\underbrace{\int_V \rho(\mathbf{r})\mathbf{r}\,d\mathbf{r}}_{=\mathbf{M}_{tot}}\cdot\mathbf{E} \tag{11}$$

For the present derivation the translational part of the total dipole moment is used ($\mathbf{M}_J = \mathbf{M}_{tot} - \mathbf{M}_D$). This simplification is only justified for the static value of the conductivity $\sigma(\omega = 0)$ as shown in section II C 2.

$$\mathcal{H}'(t) = -\mathbf{M}_J(t)\mathbf{E}(t) \quad \text{with} \quad \mathbf{M}_J(\mathbf{r}_{j,cm}(t)) = \sum_j q_j\mathbf{r}_{j,cm}(t) \tag{12}$$

Furthermore, the **Phase-Space-Probability Density** $f^{[N]}(\mathbf{r}_i, \mathbf{p}_i, t)$ is rewritten as:

$$f^{[N]}(t) = f_0^{[N]} + \Delta f^{[N]}(t) \tag{13}$$

with the condition $\Delta f^{[N]}(t = -\infty) = 0$. Consequently,

$$f^{[N]}(t = -\infty) = f_0^{[N]} = e^{-\frac{\mathcal{H}_0}{k_B T}} \tag{14}$$

which is a solution of the partial differential equation

$$\frac{\partial f_0^{[N]}}{\partial t} = \{\mathcal{H}_0, f_0^{[N]}\} \tag{15}$$

The time evolution of $f^{[N]}(t)$ is described by the **Liouville Equation**:

$$\frac{\partial f^{[N]}}{\partial t} = \{\mathcal{H}, f^{[N]}\} = -i\mathcal{L}f^{[N]} \tag{16}$$

with the Liouville Operator $\mathcal{L} := i\{\mathcal{H}, \}$.

Splitting of the terms yields

$$\frac{\partial f_0^{[N]}}{\partial t} + \frac{\partial \Delta f^{[N]}(t)}{\partial t}$$
$$= \{\mathcal{H}_0, f_0^{[N]}\} + \{\mathcal{H}_0, \Delta f^{[N]}(t)\} + \{\mathcal{H}'(t), f_0^{[N]})\} + \{\mathcal{H}'(t), \Delta f^{[N]}(t)\} \tag{17}$$

The first term of equation 17 vanishes on both sides due to equation 15 and the last term is quadratic in the perturbation (since both $\Delta f^{[N]}(t)$ and $\mathbf{E}(t)$ appear) which can be neglected according to linear response theory. Tidying up yields

$$\begin{aligned}
\frac{\partial \Delta f^{[N]}(t)}{\partial t} &= \{\mathcal{H}_0, \Delta f^{[N]}(t)\} + \{-\mathbf{M}_J(t)\mathbf{E}(t), f_0^{[N]}\} \\
&= -i\mathcal{L}_0 \Delta f^{[N]}(t) + \{f_0^{[N]}, \mathbf{M}_J(t)\}\,\mathbf{E}(t)
\end{aligned} \tag{18}$$

which has the formal solution

$$\Delta f^{[N]}(t) = e^{-i\mathcal{L}_0 t} \int\limits_0^t e^{i\mathcal{L}_0 s}\{f_0^{[N]}, \mathbf{M}_J(t)\}\,\mathbf{E}(s)\,\mathrm{d}s + A \tag{19}$$

where A is a constant which can be determined using the mentioned boundary conditions of

$$\Delta f^{[N]}(-\infty) = 0 = \int\limits_0^{-\infty} e^{-i\mathcal{L}_0(t-s)}\{f_0^{[N]}, \mathbf{M}_J(t)\}\,\mathbf{E}(s)\,\mathrm{d}s + A \tag{20}$$

(where the first exponential term in equation 19 has been taken into the integral). Flipping the limits of integration and inserting the expression for A into 19 gives:

$$\Delta f^{[N]}(t) = \int\limits_{-\infty}^t e^{-i\mathcal{L}_0(t-s)}\{f_0^{[N]}, \mathbf{M}_J(t)\}\,\mathbf{E}(s)\,\mathrm{d}s \tag{21}$$

Using the definition of the Poisson brackets, the Hamiltonian equations of motion and equation 14 the next steps become

$$\{f_0^{[N]}, \mathbf{M}_J(t)\} = \sum_{i=1}^N \left(\frac{\partial f_0^{[N]}}{\partial \mathbf{r_i}} \frac{\partial \mathbf{M}_J(t)}{\partial \mathbf{p}_i} - \frac{\partial f_0^{[N]}}{\partial \mathbf{p}_i} \frac{\partial \mathbf{M}_J(t)}{\partial \mathbf{r_i}} \right) \tag{22}$$

$$\frac{\partial f_0^{[N]}}{\partial \mathbf{r}_i} = \frac{\partial f_0^{[N]}}{\partial \mathcal{H}_0} \frac{\partial \mathcal{H}_0}{\partial \mathbf{r}_i} \qquad \text{and} \qquad \frac{\partial f_0^{[N]}}{\partial \mathbf{p}_i} = \frac{\partial f_0^{[N]}}{\partial \mathcal{H}_0} \frac{\partial \mathcal{H}_0}{\partial \mathbf{p}_i} \tag{23}$$

$$\frac{\partial f_0^{[N]}}{\partial \mathcal{H}_0} = -\frac{f_0^{[N]}}{k_B T} \tag{24}$$

$$\frac{d\mathbf{M}_J}{dt} = \sum_{i=1}^{N} \left(\frac{\partial \mathbf{M}_J}{\partial \mathbf{r}_i} \frac{d\mathbf{r}_i}{dt} + \frac{\partial \mathbf{M}_J}{\partial \mathbf{p}_i} \frac{d\mathbf{p}_i}{dt} \right) =$$
$$\sum_{i=1}^{N} \left(\frac{\partial \mathbf{M}_J}{\partial \mathbf{r}_i} \frac{\partial \mathcal{H}_0}{\partial \mathbf{p}_i} - \frac{\partial \mathbf{M}_J}{\partial \mathbf{p}_i} \frac{\partial \mathcal{H}_0}{\partial \mathbf{r}_i} \right) = \{\mathbf{M}_J, \mathcal{H}_I\} \tag{25}$$

Finally, we arrive at

$$\{f_0^{[N]}, \mathbf{M}_J(t)\} = -\frac{f_0^{[N]}}{k_B T} \{\mathcal{H}_0, \mathbf{M}_J(t)\} = \frac{f_0^{[N]}}{k_B T} \{\mathbf{M}_J(t), \mathcal{H}_0\} \tag{26}$$

and insert this into equation 21 to get

$$\Delta f^{[N]}(t) = \frac{f_0^{[N]}}{k_B T} \int_{-\infty}^{t} \mathbf{E}(s) \, e^{-i\mathcal{L}_0(t-s)} \frac{d\mathbf{M}_J}{dt} \, ds \tag{27}$$

At this point I will start up a separate track concerning our flux variable $\mathbf{J}(\mathbf{\Gamma})$ to combine it later with the ongoing derivation. It has the equilibrium ensemble average ($\mathbf{\Gamma} := (\mathbf{r}_i(t), \mathbf{p}_i(t))$ $i = 1, ..., N$):

$$\langle \mathbf{J}(\mathbf{\Gamma}) \rangle = \int_{\mathbf{\Gamma}} \mathbf{J}(\mathbf{\Gamma}) f_0^{[N]}(\mathbf{\Gamma}) \, d\mathbf{\Gamma} = 0 \tag{28}$$

Upon perturbation the average observable changes along with the phase-space-probability density giving an excess current

$$\langle \Delta \mathbf{J}(t) \rangle = \int_{\mathbf{\Gamma}} \mathbf{J}(\mathbf{\Gamma}) \Delta f^{[N]}(\mathbf{\Gamma}) \, d\mathbf{\Gamma} \tag{29}$$

where we have used equation 28. If we insert the expression for $\Delta f^{[N]}(\mathbf{\Gamma})$ in equation 27 which is the outcome of linear response theory and rearrange we obtain ($e^{-i\mathcal{L}_0(t-s)}$ is an hermitian operator with the property $Ae^{iLt}B = (e^{iLt})^* AB = e^{-iLt}AB$.):

$$\langle \Delta \mathbf{J}(t) \rangle = \int_{\mathbf{\Gamma}} \mathbf{J}(\mathbf{\Gamma}) \left(\frac{f_0^{[N]}(\mathbf{\Gamma})}{k_B T} \int_{-\infty}^{t} \mathbf{E}(s) \, e^{-i\mathcal{L}_0(t-s)} \frac{d\mathbf{M}_J}{dt} \, ds \right) d\mathbf{\Gamma}$$
$$= \frac{1}{k_B T} \cdot \int_{-\infty}^{t} \mathbf{E}(s) \, ds \int_{\mathbf{\Gamma}} e^{i\mathcal{L}_0 t} \mathbf{J}(\mathbf{\Gamma}) e^{i\mathcal{L}_0 s} \frac{d\mathbf{M}_J}{dt} f_0^{[N]}(\mathbf{\Gamma}) \, d\mathbf{\Gamma} \tag{30}$$

The operator $e^{i\mathcal{L}_0 s}$ shifts its argument, e.g. $\mathbf{M}_J$, from one point ($t = 0$) in phase space to another ($t = s$) and is therefore also called **Shift Operator**. As we have seen in (25),

$$\frac{\mathrm{d}\mathbf{M}_J}{\mathrm{d}t} = \{\mathbf{M}_J, \mathcal{H}_\prime\} = i\mathcal{L}_0\mathbf{M}_J(t) \qquad \text{with} \qquad \mathbf{M}_J(t) = e^{i\mathcal{L}_0 t}\mathbf{M}_J(0) \tag{31}$$

Now we have to make a detour to **Time Correlation Functions** which offer a tool to come closer to simulation. They can be defined as the averaged product of two observables taken at different times t' and t'', e.g. $A(\mathbf{r}, \mathbf{p}, t')$ and $B(\mathbf{r}, \mathbf{p}, t'')$. The equilibrium average, indicated as a subscript, can be taken over time (32) or over the phase-space (33) if we assume the **Ergodic Theorem** to be valid:

$$\langle A(t')B(t'')\rangle_{equ} = \lim_{\tau\to\infty} \frac{1}{t} \int_0^\infty A(t'+t)B(t''+t)\,\mathrm{d}t \tag{32}$$

$$\langle A(t')B(t'')\rangle_{equ} = \int_{\mathbf{\Gamma}} f_0^{[N]}(\mathbf{\Gamma}, t)B^*(\mathbf{\Gamma})e^{i\mathcal{L}_0(t'-t'')}A(\mathbf{\Gamma})\,\mathrm{d}\mathbf{\Gamma}$$

$$= \int_{\mathbf{\Gamma}} f_0^{[N]}(\mathbf{\Gamma}, t)e^{i\mathcal{L}_0 t''}B^*(\mathbf{\Gamma})e^{i\mathcal{L}_0 t'}A(\mathbf{\Gamma})\,\mathrm{d}\mathbf{\Gamma} \tag{33}$$

As alluded to in the previous section, computer simulations cannot reach the limit infinity but the relation is satisfyingly fulfilled for times of length τ being longer than the period of fluctuation. From the Ergodic Theorem follows also the time-invariance of correlation functions:

$$\langle A(t')B(t'')\rangle_{equ} = \langle A(t'+\tau)B(t''+\tau)\rangle_{equ} \qquad \text{for any} \quad \tau \tag{34}$$

$$= \langle A(t)B(0)\rangle_{equ} \quad \text{and} \quad \tau = -t'' \tag{35}$$

In the following the subscript for equilibrium correlation functions will be dropped since there is no ambiguity. It is now easy to see the analogy in equation (30) and rewrite the correlation function in more compact form. Furthermore, we introduce a timeshift in the correlation function which is justified above, we divide by the volume to create intensive variables, and we divide by 3 since we take the average of the product of the 3 components of vectors.

$$\frac{\langle \Delta \mathbf{J}(t) \rangle}{V} = \frac{1}{3Vk_BT} \cdot \int\limits_{-\infty}^{t} \mathbf{E}(s) \, \langle \mathbf{J}(t) \frac{\mathrm{d}\mathbf{M}_J(s)}{\mathrm{d}t} \rangle \, \mathrm{d}s \tag{36}$$

$$= \frac{1}{3Vk_BT} \cdot \int\limits_{-\infty}^{t} \mathbf{E}(s) \, \langle \mathbf{J}(t)\mathbf{J}(s) \rangle \, \mathrm{d}s \tag{37}$$

Taking the Fourier-transformation of $\mathbf{E}(s)$ (which is spatially homogeneous and thus independent of $\mathbf{r}$) and picking only one term ($\omega_k = \omega_0$) for representation yields

$$\mathbf{E}(s) = \int\limits_{-\infty}^{\infty} \tilde{\mathbf{E}}(\omega)e^{-i\omega s} \, \mathrm{d}\omega \approx \sum_{\omega_k} \tilde{\mathbf{E}}(\omega_k)e^{-i\omega_k s} \tag{38}$$

so equation 37 becomes:

$$\frac{\langle \Delta \mathbf{J}(\omega_0)e^{-i\omega_0 s} \rangle}{V} = \frac{1}{3Vk_BT} \tilde{\mathbf{E}}(\omega_0) \int\limits_{-\infty}^{t} e^{-i\omega_0 s} \, \langle \mathbf{J}(t-s)\mathbf{J}(0) \rangle \, \mathrm{d}s \tag{39}$$

Next, we exchange the integration variable $t' = t - s$ so that $\mathrm{d}t' = -\mathrm{d}s$, the sign changes, the lower and upper limit change to 0 and ∞, respectively, and $e^{-i\omega s} = e^{i\omega t}e^{-i\omega s - t} = e^{-i\omega t}e^{i\omega t'}$:

$$\frac{\langle \Delta \mathbf{J}(\omega_0)e^{-i\omega_0 s} \rangle}{V} = \frac{1}{3Vk_BT} \tilde{\mathbf{E}}(\omega_0)e^{-i\omega_0 t} \int\limits_{0}^{\infty} e^{i\omega t'} \, \langle \mathbf{J}(t')\mathbf{J}(0) \rangle \, \mathrm{d}t' \tag{40}$$

to finally obtain by writing ω and $\mathbf{E}$ instead of ω_0 and $\tilde{\mathbf{E}}$

$$\frac{\langle \Delta \mathbf{J}(\omega) \rangle}{V} = \frac{1}{3Vk_BT} \mathbf{E}(\omega) \int\limits_{0}^{\infty} e^{i\omega t'} \, \langle \mathbf{J}(t')\mathbf{J}(0) \rangle \, \mathrm{d}t' \tag{41}$$

or

$$\frac{\langle \Delta \mathbf{J}(\omega) \rangle}{V} = \sigma(\omega)\mathbf{E}(\omega) \quad \text{with} \quad \sigma(\omega) = \frac{1}{3Vk_BT} \int\limits_{0}^{\infty} e^{i\omega t} \langle \mathbf{J}(t)\mathbf{J}(0) \rangle \, \mathrm{d}t \tag{42}$$

where $\sigma(\omega)$ represents the conductivity. The second equation in (42) is just the Green-Kubo formula for the charge transport. Also, substituting $\mathbf{E}$ for any other field and $\mathbf{J}$ the conjugate flux, the corresponding transport coefficient can be calculated.

2. Additional Notes on the Green-Kubo Formula for Ionic Liquids

Ionic liquids combine two important features which have already been mentioned and which make ILs so unique: The molecules have a net charge, per definition of an ion, and a non-uniform electron distribution which makes them polar. On the macroscopic level, ILs therefore exhibit properties of both a conducting and a dielectric medium. This becomes manifest in non-zero values for both the collective translational dipole moment $\mathbf{M}_J$ and rotational dipole moment $\mathbf{M}_D$

$$\mathbf{M}_{tot} = \sum_j \sum_\alpha q_{j,\alpha} \mathbf{r}_{j,\alpha} \tag{43}$$

$$= \sum_j \sum_\alpha q_{j,\alpha} (\mathbf{r}_{j,\alpha} - \mathbf{r}_{j,cm} + \mathbf{r}_{j,cm}) \tag{44}$$

$$= \underbrace{\underbrace{\sum_j \sum_\alpha q_{j,\alpha} (\mathbf{r}_{j,\alpha} - \mathbf{r}_{j,cm})}_{\mu_j} + \underbrace{\sum_j q_j \mathbf{r}_{j,cm}}_{\mathbf{M}_J}}_{\mathbf{M}_D} \tag{45}$$

with $\mathbf{r}_{j,\alpha}$ and $q_{j,\alpha}$ being the positional vector and partial charge of the α's atom of the jth molecule and $\mathbf{r}_{j,cm}$ being the positional vector of the center of mass of the jth molecule.

Clearly, an electric field applied to a IL-system triggers both conduction and polarization which influence each other. Therefore the response of an IL system to an external field is more properly described by the macroscopic polarization $\mathbf{M}_{tot}$ and the "transport coefficient" $\Sigma(\omega)$, the generalized dielectric constant.

$$\frac{\langle \mathbf{M}_{tot} \rangle_E}{V} = \frac{\Sigma(\omega)}{4\pi} \cdot \mathbf{E}(\omega) \tag{46}$$

As stated above, the Green-Kubo relation applies to all transport processes including this one and a derivation for the exact expression in terms of correlation functions would run analogously but with much more terms. Also, this equation includes 4π to use SI units and the total dipole moment $\mathbf{M}_{tot}$. The outcome can be merged to[12,13]

$$\Sigma(\omega) = \epsilon(\omega) - 1 + \frac{4\pi i \sigma(\omega)}{\omega} \tag{47}$$

where the conductivity has the expanded form

$$\sigma(\omega) = \frac{1}{3Vk_BT} \int\limits_0^\infty e^{i\omega t} \langle \mathbf{J}(0)\mathbf{J}(t) \rangle \, \mathrm{d}t + \frac{i\omega}{3Vk_BT} \int\limits_0^\infty e^{i\omega t} \langle \mathbf{M}_D(0)\mathbf{J}(t) \rangle \, \mathrm{d}t \tag{48}$$

This has the important consequence that the conductivity of ionic liquids is also determined by the coupling between the collective rotational dipole moment and current. Even so, the coupling term vanishes in the zero frequency limit, i.e. for the static conductivity, where equation 48 equals 42.

3. Einstein-Helfand Formula

The Einstein-Helfand formula relates the mean square displacement of $\mathbf{M}_J$ to the static conductivity and is therefore a valuable independent way to evaluate the results of calculations using the Green-Kubo relation. Nevertheless, it is possible to derive the first from the latter[14] which proves the internal consistency within the theoretic foundations used.

The collective translational dipole moment can be converted to the collective current via

$$\mathbf{M}_J(\mathrm{r}_{j,cm}(t)) = \sum_j q_j \mathbf{r}_{j,cm}(t) = \sum_j \int\limits_0^t q_i \frac{\mathrm{d}\mathbf{r}_{j,cm}(t)}{\mathrm{d}t} \, \mathrm{d}t$$
$$= \sum_i \int\limits_0^t q_i \mathbf{v}_i(t) \, \mathrm{d}t = \int\limits_0^t \mathbf{J}(\mathbf{v}_i(t)) \, \mathrm{d}t \tag{49}$$

and (A function $\mathbf{F}(\mathrm{x}_i(t))$ is denoted as $\mathbf{F}(t)$ for convenience.)

$$\langle \Delta \mathbf{M}_J(t)^2 \rangle = \langle (\mathbf{M}_J(t) - \mathbf{M}_J(0))(\mathbf{M}_J(t) - \mathbf{M}_J(0)) \rangle$$
$$= 2 \langle \int\limits_0^t \mathrm{d}t' \mathbf{J}(t') \int\limits_0^t \mathrm{d}t'' \mathbf{J}(t'') \rangle = 2 \int\limits_0^t \mathrm{d}t' \int\limits_0^{t'} \mathrm{d}t'' \langle \mathbf{J}(t')\mathbf{J}(t'') \rangle \tag{50}$$
$$= 2 \int\limits_0^t \mathrm{d}t' \int\limits_0^{t'} \mathrm{d}t'' \langle \mathbf{J}(t'-t'')\mathbf{J}(0) \rangle$$

Changing the variables to $y = t' - t''$ which has the limits $(t'', 0)$ and $x = t''$ gives

$$2 \int\limits_0^t \mathrm{d}x \int\limits_0^x \mathrm{d}y \, \langle \mathbf{J}(y)\mathbf{J}(0) \rangle \tag{51}$$

Now we define

$$u(x) = \int\limits_0^x \mathrm{d}y \, \langle \mathbf{J}(0)\mathbf{J}(y) \rangle \tag{52}$$

and integrate (51) by parts

$$2 \int\limits_0^t \mathrm{d}x \, 1 \cdot u(x) = 2 \left(x \, u(x) \Big|_0^t - \int\limits_0^t x \, \frac{\mathrm{d}u(x)}{\mathrm{d}x} \, \mathrm{d}x \right)$$

$$= 2 \left(t \, u(t) - \int\limits_0^t x \, \langle \mathbf{J}(x)\mathbf{J}(0) \rangle \, \mathrm{d}x \right)$$

$$= 2 \left(t \int\limits_0^x \mathrm{d}y \, \langle \mathbf{J}(0)\mathbf{J}(y) \rangle - \int\limits_0^t x \langle \mathbf{J}(x)\mathbf{J}(0) \rangle \, \mathrm{d}x \right) \tag{53}$$

If we integrate the second term of (53) by parts as well and take advantage of general properties of time correlation functions (33) we get

$$-\int\limits_0^\infty x \langle \mathbf{J}(x)\mathbf{J}(0) \rangle \, \mathrm{d}x = \underbrace{t \langle \mathbf{M}_J(0)\mathbf{J}(t) \rangle \Big|_0^\infty}_{\stackrel{!}{=} 0} - \int\limits_0^\infty \langle \mathbf{M}_J(0)\mathbf{J}(t) \, \mathrm{d}t$$

$$= -\langle \mathbf{M}_J(0)\mathbf{M}_J(t) \rangle \Big|_0^\infty = \langle \mathbf{M}_J^2 \rangle \tag{54}$$

With an exchange of x for t for clarity and taking the limit $t \to \infty$ we approach our goal

$$\lim_{t \to \infty} \langle \Delta \mathbf{M}_J(t)^2 \rangle = 2 \left(t \int\limits_0^\infty \langle \mathbf{J}(t)\mathbf{J}(0) \rangle \, \mathrm{d}t + \langle \mathbf{M}_J^2 \rangle \right) \tag{55}$$

which is rearranged to the Einstein-Helfand formula for conductivity when compared to equation 42

$$\sigma(\omega = 0) = \frac{1}{6Vk_BT} \lim_{t \to \infty} \frac{\langle \Delta \mathbf{M}_J(t)^2 \rangle - 2\langle \mathbf{M}_J^2 \rangle}{t}$$

$$= \frac{1}{6Vk_BT} \lim_{t \to \infty} \frac{\langle \Delta \mathbf{M}_J(t)^2 \rangle}{t}$$

$$= \frac{1}{3Vk_BT} \int\limits_0^\infty \langle \mathbf{J}(t)\mathbf{J}(0) \rangle \, \mathrm{d}t \tag{56}$$

26

4. Nernst-Einstein Formula

Here, only the expression for binary ILs with monovalent ions is given.

As already stated the Nernst-Einstein equation is a single particle approximation for the current neglecting any interactions among the particles, i.e. the cross terms with $i \neq j$ are simply left out. Terms where particle i is not from the same ion species as j would contribute most. Furthermore, we assume that the mean square displacement $\langle \Delta \mathbf{r}_{j,cm}(t)^2 \rangle$ is equal for all particles of a single ion species. Thus we simplify the mean square displacement of the collective translational dipole moment with

$$\Delta \mathbf{M}_J(t)^2 = (\mathbf{M}_J(t) - \mathbf{M}_J(0))^2 \tag{57}$$

$$= [\sum_j^N q_j(\mathbf{r}_{j,cm}(t) - \mathbf{r}_{j,cm}(0))][\sum_i^N q_i(\mathbf{r}_{i,cm}(t) - \mathbf{r}_{i,cm}(0))] \tag{58}$$

$$\approx \sum_j^N q_j^2(\mathbf{r}_{j,cm}(t) - \mathbf{r}_{j,cm}(0))^2 = \sum_j^N q_j^2 \Delta \mathbf{r}_{j,cm}(t)^2 \tag{59}$$

$$\approx \frac{N}{2} q_+^2 \Delta \mathbf{r}_{cm,+}(t)^2 + \frac{N}{2} q_-^2 \Delta \mathbf{r}_{cm,-}(t)^2 \tag{60}$$

$$= n_+ q_+^2 \Delta \mathbf{r}_{cm,+}(t)^2 + n_- q_-^2 \Delta \mathbf{r}_{cm,-}(t)^2 \tag{61}$$

with $n = N/2$ the amount of particles of one ion species. Now, the diffusion coefficient being the transport coefficient for particle flux can be expressed by Green-Kubo and Einstein-Helfand equations in an analogous way to the conductivity:

$$D = \lim_{t \to \infty} \frac{\langle \Delta \mathbf{r}(t)^2 \rangle}{6t} \tag{62}$$

The conductivity is consequently written as

$$\sigma(\omega = 0) \approx \frac{1}{6V k_B T} \lim_{t \to \infty} \frac{n_+ q_+^2 \Delta \mathbf{r}_{cm,+}(t)^2 + n_- q_-^2 \Delta \mathbf{r}_{cm,-}(t)^2}{t} \tag{63}$$

$$= \frac{1}{V k_B T} (n_+ q_+^2 D_+ + n_- q_-^2 D_-) \tag{64}$$

which is just the Nernst-Einstein relation as in equation 6 with $q = ze$.

III. METHODS

Several programs have been devised with the programming language FORTRAN90 to analyze trajectories of the IL-systems [bmim][bf4], [bmim][pf6], [bmim][tfa], [emim][cla], [emim][trif], [emim][dcyi], and [evot][dcyi], making use of the formulas described in the Theory section (See table I for explanation of the acronyms.). The system [evot][dcyi] is only different from [emim][dcyi] in that the charge distribution is different. This is in order to show up the influence of electrostatic forces, i.e. charge variation.

The computation of the trajectories themselves with the molecular dynamics program CHARMM (Chemistry at **Har**vard **M**olecular **M**echanics[15,16]) was not part of this thesis and is described in Ref. 17, 18, and 19.

The implemented algorithms are presented here in a meta language resembling FORTRAN90: Variables and arrays of variables are written small lettered, looping and branching statements, as well as subroutines are noted in capitals. Variables in parenthesis after arrays of variables indicate the dimensions of the array. Tables II, III, and IV explain the meaning of the variables.

Unfortunately, many branches were included due to technical constraints. In terms of computation time, this affected the calculation of the mean square displacement at most.

Acronym	IUPAC name
[bmim]	1-butyl-3-methylimidazolium
[emim]	1-ethyl-3-methylimidazolium
[evot]*	1-ethyl-3-methylimidazolium
[bf4]	Tetrafluoroborate
[cla]	Chloride
[dcyi]	Dicyanimide
[pf6]	Hexafluorophosphate
[tfa]	Trifluoroacetate
[trif]	Trifluoromethanesulfonate (Triflate)

TABLE I: Acronyms and their full IUPAC name. All IL interactions are parametrized according to Ref. 20. *: For [evot] the charge distribution from Ref. 21 is taken.

variable	meaning
corrsteps	# of timesteps of the MSD, MSDMJ, VACF, or CACF
timesteps	# of coordinateframes of a trajectory to use
inputunit_1	unit with trajectory
natom	# of atoms
nmol	# of molecules
rcom_1	center-of-mass position vector
msd_cation, msd_anion	mean square displacement
timestep	length of timestep in picoseconds

statement	meaning
REWIND	start reading a trajectory from the beginning
READFRAME	read the coordinates for one timestep from the trajecotry
CALCULATE	calculate subsequent variable

TABLE II: Description of variables and statements of the following algorithms.

A. Mean Square Displacement

1. MSD_A

Algorithm 1 MSD_A

```
DO t = 1, corrsteps
  REWIND(inputunit_1,inputunit_2)
  DO n = 1, timesteps - t + 1
    READFRAME(inputunit_1)
    IF (n = 1) THEN
      DO l = 1, t
        READFRAME(inputunit_2)
      END DO
    ELSE IF
      READFRAME(inputunit_2)
    END IF
    DO i = 1, natom
      CALCULATE rcom_1(nmol,3)
      CALCULATE rcom_2(nmol,3)
      IF (i = natom) THEN
        msd_cation(t) = msd_cation(t) + (rcom_1 - rcom_2)**2
        msd_anion(t)  = msd_anion(t)  + (rcom_1 - rcom_2)**2
      END IF
    END DO
  END DO
END DO
DO t = 1, corrsteps
  msd_cation(t) = msd_cation(t) / nion
  msd_anion(t)  = msd_anion(t)  / (timesteps - t + 1)
  WRITE t*timestep, msd_cation(t), msd_anion(t)
END DO
```

2. MSD_B

variable	meaning
readlength	# of timesteps to read from trajectory
iframe	time interval of MSD
diffusion	mean square displacement
ionspecies	cation or anion
nion	# of molecules of an ionspecies

TABLE III: Description of the variables of the MSD_B algorithm.

Algorithm 2 MSD_B

```
DO t = 1, readlength
  READFRAME(inputunit_1)
  CALCULATE rcom_1(inputunit_1,nmol)
  REWIND(inputunit_2)
  DO u = 1, t
    READFRAME(inputunit_2)
    CALCULATE rcom_2(inputunit_2, nmol)
    iframe = t - u + 1
    diffusion(ionspecies, iframe) =
                diffusion(ionspecies, iframe)
              + DOTPRODUCT((rcom_1 - rcom_2),(rcom_1 - rcom_2))
              / (readlength - iframe + 1)
  END DO
END DO
DO i = 1, readlength
  WRITE j*timestep, diffusion(ionspecies, i)/nion
END DO
```

B. Mean Square Displacement of the Collective Translational Dipole Moment

1. Mjmj

variable	meaning
charge	net charge of a molecule
mj	collective translational dipole moment
mjmj	mean square displacement of mj

TABLE IV: Description of the variables of the Mjmj algorithm.

Algorithm 3 MJMJ

```
DO t = 1, timesteps
  READFRAME
  DO i = 1, natom
    CALCULATE rcom(nmol)
    mj(t) = mj(t) + charge(nmol) * rcom(nmol)
  END DO
  IF (t = corrsteps)
    DO j = 1, corrsteps
      mjmj(k) = mjmj(k) +  (mj(1) - mj(t))**2
      END DO
      DO j = 1, (corrsteps - 1)
      mj(t) = mj(t+1)
      END DO
      mj(corrsteps) = 0
  END IF
END DO
DO t = 1, corrsteps
  mjmj(t) = mjmj(t) / (timesteps + 1 - corrsteps)
  WRITE t * timestep, mjmj(t)
END DO
```

C. Auto-Correlation Function

The program CORREL_VELCM uses routines written by C. Schröder and G. Neumayr which allow to correlate the time-series of dynamic variables. Moreover, they provide methods to refine the outcome by averaging ("Running Average"), application of filters ("Savitzky-Golay", "High-Pass", "Low-Pass"), and correlation, all in Fourier space. The "Running Average", RAVG, method was used for the results described here. The value after RAVG indicates the range of the interval in fourier space for which the average was taken (e.g. RAVG30 averaged an interval of 30 frequencies).

IV. RESULTS AND DISCUSSION

In this section, the conductivity, and as an intermediate product also the diffusion coefficient, of a variety of ionic liquids are presented, compared to experimental values, and eventually discussed. Results are summarized in table XI and XX.

A. Diffusion Coefficient

1. Diffusion Coefficient from the Green-Kubo Formula

a. [bmim][bf4] The diffusion coefficient of the IL system [bmim][bf4] was determined using the Green-Kubo formula (equation 42) and by inserting this into the Nernst-Einstein relation (equation 63) the conductivity was estimated.

First, the velocity auto-correlation functions (VACF) were calculated for a 8200ps segment of the trajectory with the CHARMM-module CORREL, and the program COR-REL_VELCM, and integrated with the program PERLINT (The CHARMM-module and the CORREL_VELCM program produced exactly the same results.). Unfortunately, the single particle VACF decays slowly due to the cooperative effect of ILs[6]. Thus the long-time tail of the VACF contributes significantly to the integral and in consequence to the diffusion coefficient. The strong noise exacerbates the situation in that a very good statistic is necessary. Figure 1 displays the correlation functions and the corresponding integrals for the cation, bmim, and the anion, bf4, respectively.

Two points immediately attract attention, the already mentioned high noise troughout the function and its integral, and the increase of the noise towards the end. The rise stems from the decrease of statistics of long-time correlations. Furthermore, the system [bmim][bf4] is highly viscous and the calculated viscosity from the very same data even overestimates the experimental value[18]. This resistance to flow is reflected less in the decay of the VACF than in the need for calculation over an extended time-interval and better statistics[6].

Some groups fit the integral of the VACF to an exponential decay function as it would be predicted by kinetic theory to extract a reliable diffusion coefficient[22],[5]. Here, I just calculated the mean value of the integral for $1000ps < t < 7000ps$ which turned out to be $(9.4\pm1.1)\cdot10^{-6}e^2\AA^2 AKMA^{-1}$ for the cation, and $(9.0\pm1.3)\cdot10^{-6}e^2\AA^2 AKMA^{-1}$ for the anion ($AKMA$ is the internal time-unit of CHARMM. $1AKMA = 0.04888ps$ or $20AKMA \approx 1ps$).

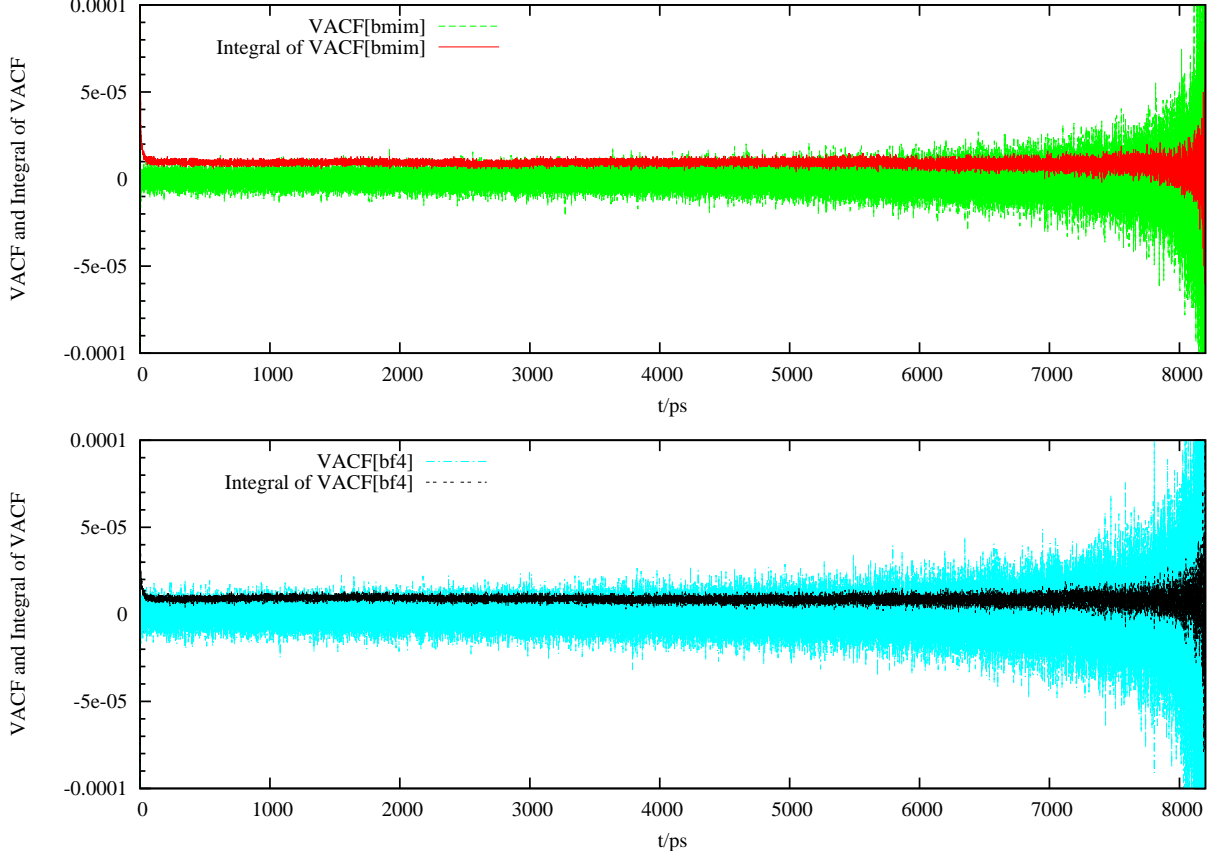FIG. 1: VACF ($\langle\mathbf{v}(0)\mathbf{v}(t)\rangle/\mathring{A}^2 AKMA^{-2}$) and its integral ($\int\langle\mathbf{v}(0)\mathbf{v}(t)\rangle\mathrm{d}t/\mathring{A}^2 AKMA^{-2}ps$) for the cation [bmim], and anion [bf4] for 8200ps.

Figure 2 displays arbitrarily chosen close-ups of the VACFs and VACF-integrals where one can clearly see that the integral has converged and consequently remains constant.

The diffusion constants and the conductivity according to the Nernst-Einstein relation are given in table V. These values are in rough accordance with those of MSD-, CACF- and MSDMJ-calculations (see sections IV A 2, IV B 1, and IV B 2) and of other groups[23],[24] (see table XI). Moreover, the conductivity calculated from diffusion coefficients, $\sigma_{NE} = 4.8$ is higher by a factor 1.5 than those calculated from collective properties $\sigma_{GK} = 3.2$ which is expected in theory (section II) and visualized in figure 4.

Ion	D_{GK}
[bmim]	1.31
[bf4]	1.26

TABLE V: Diffusion coefficients calculated with the Green-Kubo formula ($D_{GK}/10^{-7}cm^2s^{-1}$).
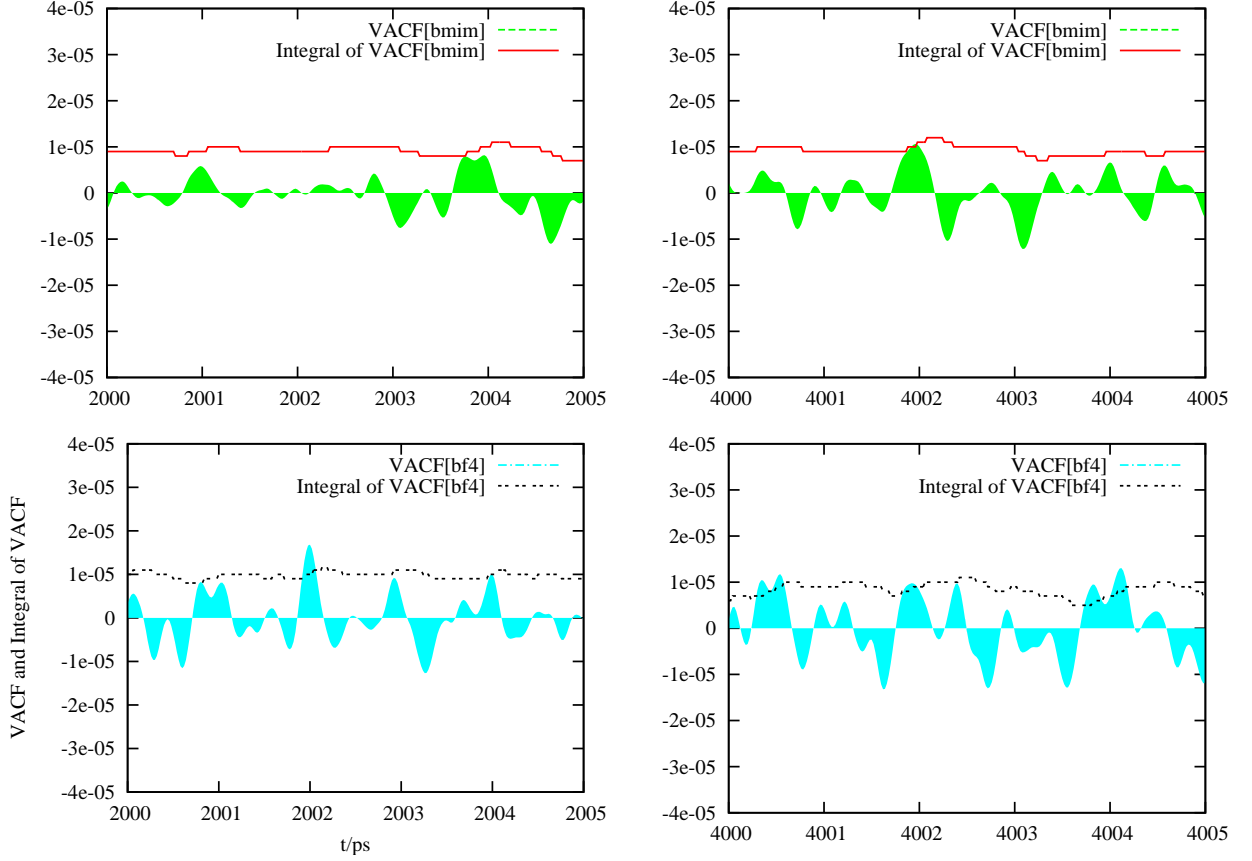
FIG. 2: VACF ($\langle \mathbf{v}(0)\mathbf{v}(t)\rangle / \mathring{A}^2 AKMA^{-2}$) and its integral ($\int \langle \mathbf{v}(0)\mathbf{v}(t)\rangle \mathrm{d}t / \mathring{A}^2 AKMA^{-2}ps$) for the cation [bmim] for two arbitrarily chosen segments. The area beneath the velocity auto-correlation function is filled to depict its and its integral's fluctuations.

To extract information on the molecular motion figure 3 zooms in on the initial 10ps of the VACFs and integrals of both the anion and the cation and figure 4 compares the normalized summed VACFs to the current auto-correlation function (CACF.) The shape of the VACF in figure 3 can be interpreted quite straightforward: The initial value at $t = 0ps$ stands for the mean square velocity of the ion. The values for $\langle v^2 \rangle$ are given in the table VI. A following steep decay and minimum with negative values reflect that the ion soon collides with others and consequently moves in an opposite direction. The minimum is thus the average time until the first collision of a molecule which is about 0.2 to 0.3ps for both ions which is typical for condensed phases[22]. These and density distribution functions suggest that the ion is surrounded by a cage built up of other molecules[4].

Accordingly, the subsequent rise and fall into a second trough point to a second and a

38

Ion	$\langle \mathbf{v}^2 \rangle / \mathring{A}^2 AKMA^{-2}$	$\langle \mathbf{v}^2 \rangle / \mathring{A}^2 ps^{-2}$
[bmim]	$1.6 \cdot 10^{-4}$	0.067
[bf4]	$4.0 \cdot 10^{-4}$	0.17

TABLE VI: Mean square velocity of [bmim][bf4].

third collision within the cage if the cage itself hasn't disassembled by then. Such long-lived cage structures are also suggested by density distribution functions. The VACF of [bmim] appears somewhat damped compared to the VACF of [bf4] which most probably goes along with the cation's bigger size and mass. The values for the diffusion constant (see table V) are in the expected order of magnitude but too rough to allow any comparisons. The inset in figure 3 zooms in on the following course of the correlation functions and their integrals which decay fairly quickly into a random noise pattern and converge, respectively.

The normalized single particle velocity and collective current auto-correlation functions in figure 4 permit a direct, unit-independent comparison and indicate the link between conductivity and diffusion as manifested in the Nernst-Einstein relation. As already stated on page 17 the difference between the single particle and collective property auto-correlation functions are due to the cross-correlations between different single particles figure 4. For instance, if a pair of oppositely charged ions moves in the same direction it contributes to the diffusion coefficient but not to the conductivity. If cross-correlations were negligible the normalized velocity and current auto-correlation functions were expected to coincide. Closer inspection of figure 4 also shows that the VACF is smoother than the CACF. As a general rule, single particle property functions feature better statistics since it is possible to average over all particles as opposed to collective property functions. This is also reflected when comparing MSD with MSDMJ (sections IV A 2 and IV B 2).
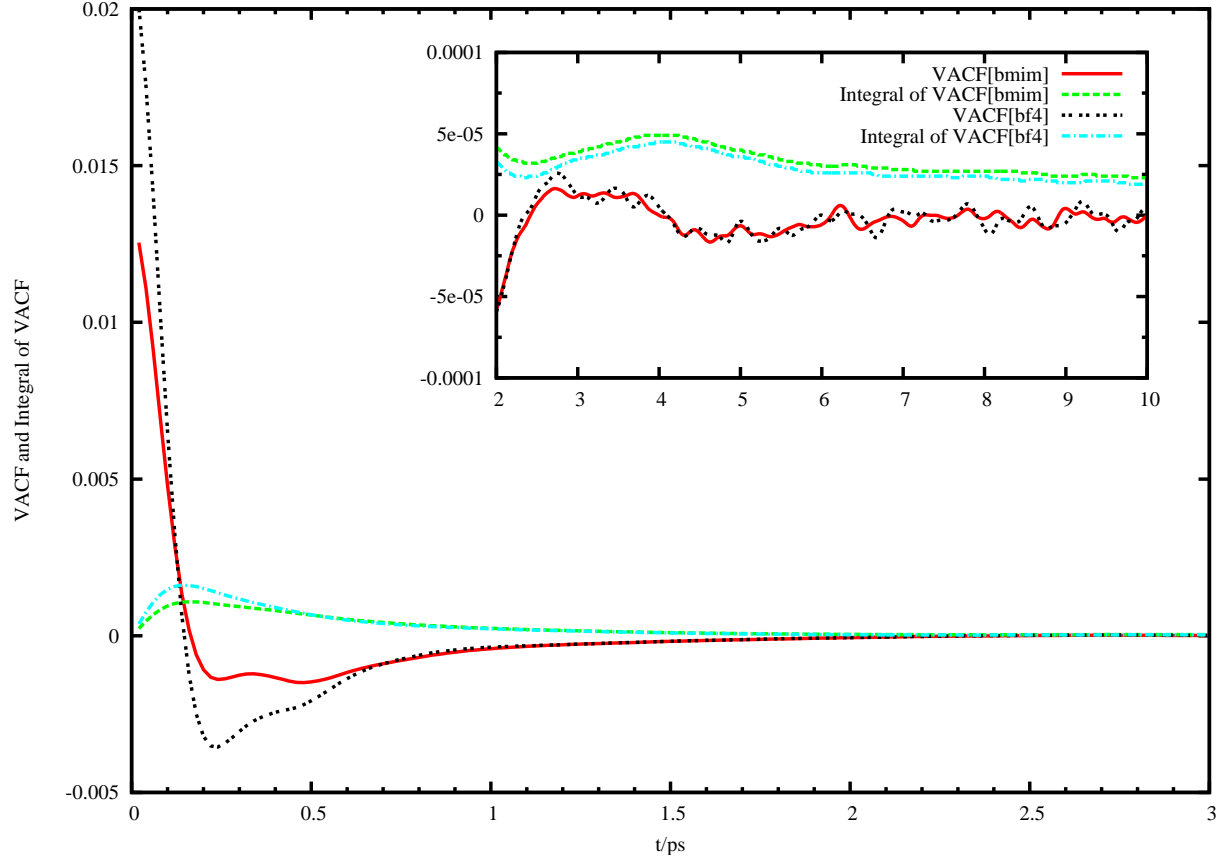
FIG. 3: VACF ($\langle \mathbf{v}(0)\mathbf{v}(t)\rangle / \mathring{A}^2 AKMA^{-2}$) and its integral ($\int \langle \mathbf{v}(0)\mathbf{v}(t)\rangle \mathrm{d}t / \mathring{A}^2 AKMA^{-2}ps$) for the cation [bmim] and the anion [bf4] for the first 5ps.
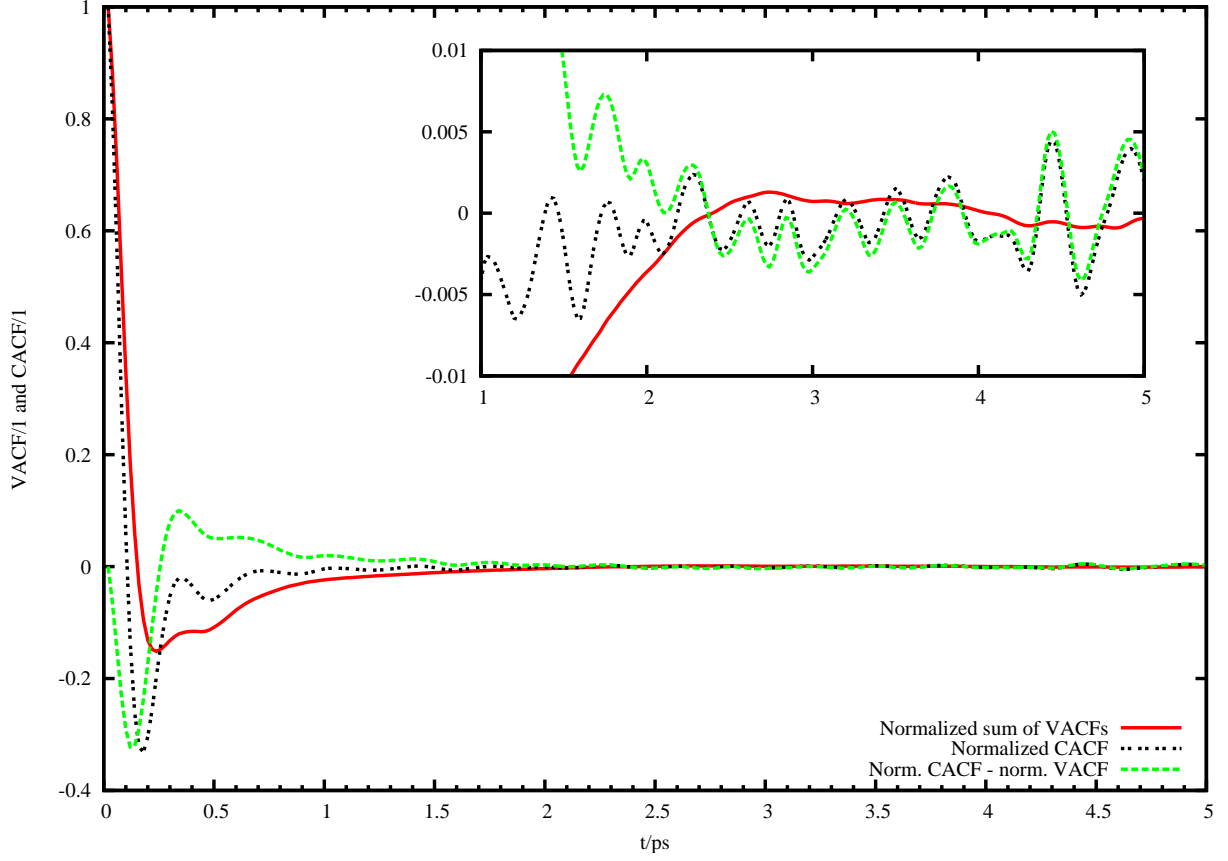
FIG. 4: Normalized sum of the VACFs $((\langle \mathbf{v}_+(t)\mathbf{v}_+(0)\rangle + \langle \mathbf{v}_-(t)\mathbf{v}_-(0)\rangle)/\langle \mathbf{v}^2\rangle)$ and normalized CACF $(\langle \mathbf{J}(0)\mathbf{J}(t)\rangle/\langle \mathbf{J}^2\rangle)$ for the first 5ps, as well as their difference $(\langle \mathbf{J}(0)\mathbf{J}(t)\rangle/\langle \mathbf{J}^2\rangle - (\langle \mathbf{v}_+(t)\mathbf{v}_+(0)\rangle + \langle \mathbf{v}_-(t)\mathbf{v}_-(0)\rangle)/\langle \mathbf{v}^2\rangle)$. The inset zooms in on the tail of the correlation functions.

2. Diffusion Coefficient from the Einstein Relation

The mean square displacement (MSD) was calculated with the program MSD_A and MSD_B (using equation (62)) for the trajectories of the following IL systems: [bmim][bf4], [bmim][pf6], [bmim][tfa], and [emim][cla]. The gradient of the MSD is proportional to the diffusion coefficient (equation 62) and can be calculated by linear regression of the linear part of the MSD curve. The linear regression (LR) is generally included to highlight the linear part.

a. [bmim][bf4] Calculated diffusion coefficients from the gradient of MSD-curves are listed in table VII. For D_{100ps} I used MSD_A and averaged the MSD of 142 100ps-trajectory slices whereas for D_{400ps} I took MSD_B and and a single 4000ps-trajectory slice. The statistics become worse versus the end for all MSD-curves although less pronounced for the 100ps-MSD-curve for which the sample was larger (cf. figure 5).

Remarkably, the slope for the short 100ps-MSD turns out to be flatter than for the 400ps-MSD which isn't the case for [emim][cla] nor for MSDMJ calculations. However, the longer MSD curve evaluates to a more accurate diffusion coefficient when compared with experimental values from literature (Ref. 23, and 24, see table XI). Compared with the results from the Green-Kubo formula, the MSD misses the diffusion coefficient by one third to two thirds. Also, the diffusion coefficient of the heavier and bigger cation is higher just as already reported in literature.

Ion	D_{400ps}
[bmim]	0.94
[bf4]	0.61

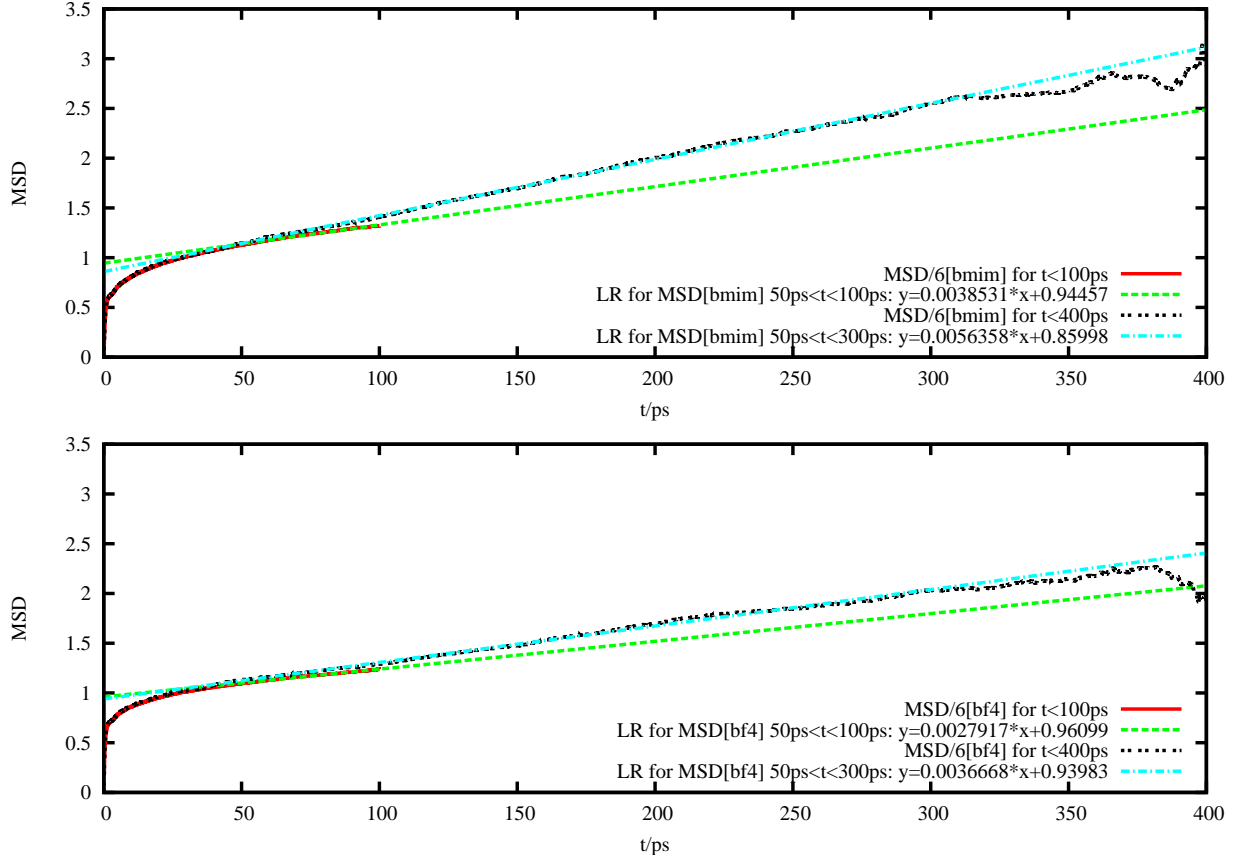TABLE VII: Diffusion coefficients ($D/10^{-7}cm^2s^{-1}$)).

FIG. 5: **[bmim][bf4]**: MSD ($\langle \Delta \mathbf{r}(t)^2 \rangle / \mathring{A}^2$) of the cation, [bmim], and the anion, [bf4]. The linear regression (LR) for the most linear part (as deduced by visual inspection) is included as well.

b. *[bmim][pf6]* Calculated diffusion coefficients are listed in table VIII. The MSD of 49 200ps-trajectory slices were calculated (using MSD_A) and averaged which is plotted in figure 6. Again, the increased rippling at the 200ps end of the curves are due to smaller sampling of long time MSD values.

As for the [bmim][bf4] system, the calculated diffusion coefficients are close to results of Ref. 23, 24 and 25 (also see table XI), and obviously the heavier and bigger cation migrates faster.

Ion	D_{200ps}
[bmim]	0.40
[pf6]	0.21

TABLE VIII: Diffusion coefficients $D/10^{-7}cm^2s^{-1}$.
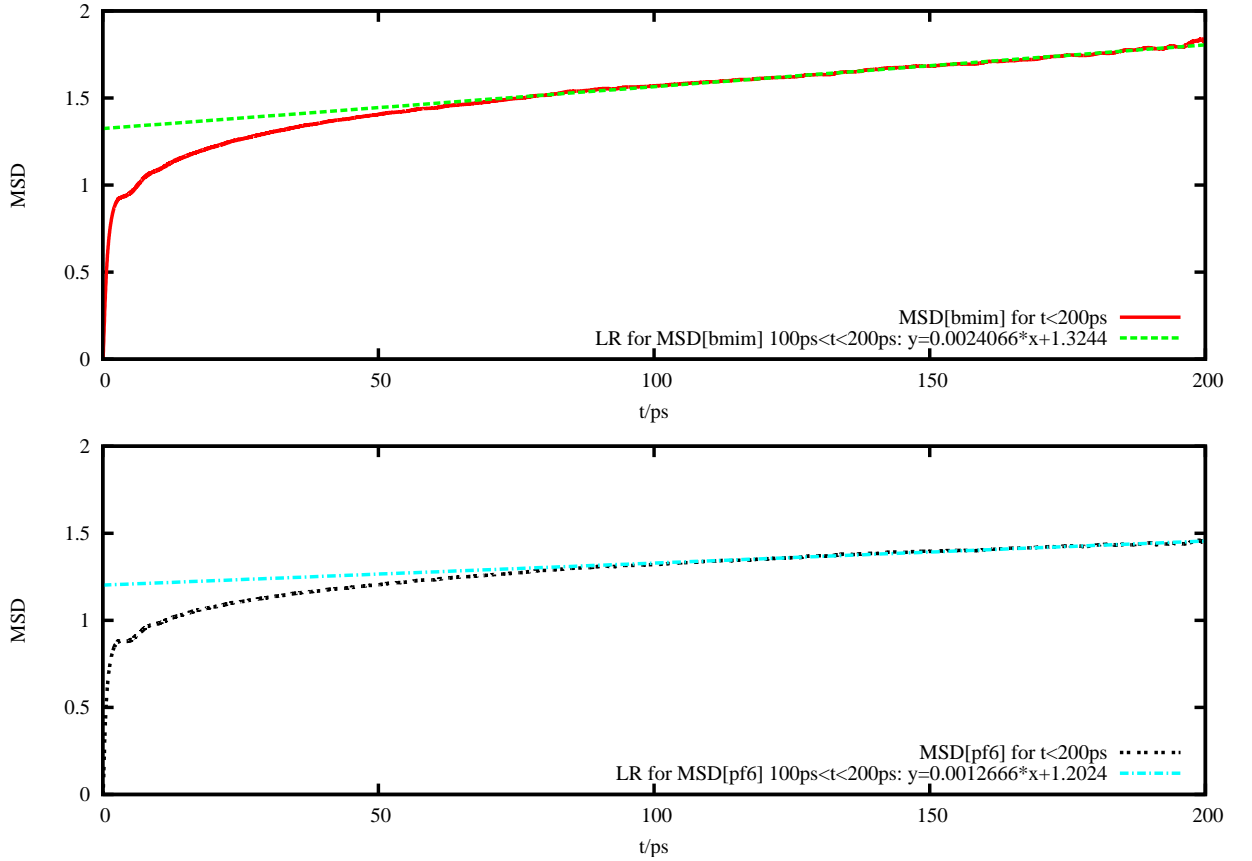
FIG. 6: **[bmim][pf6]**: MSD ($\langle \Delta \mathbf{r}(t)^2 \rangle / \mathring{A}^2$) of the cation, [bmim], and the anion, [pf6]. The linear regression (LR) for the most linear part (as deduced by visual inspection) is included as well.

c.   [bmim][tfa]   Calculated diffusion coefficients are listed in table X. The MSD of 250 400ps-trajectory slices were calculated for 100ps (using MSD_A), averaged, and plotted in figure 7. Here, the "Sliding Window" averaging of MSD_A gave rise to a smooth curve until the end.

The 100ps-MSD curve is fairly short and it is to be expected that the linear part hasn't begun within that time and the gradient is still to steep. Therefore, the calculated diffusion coefficients are most likely overestimated. This is confirmed by comparison with experimental data from Ref. 24 (table XI).

Ion	D_{100ps}
[bmim]	2.3
[tfa]	2.5

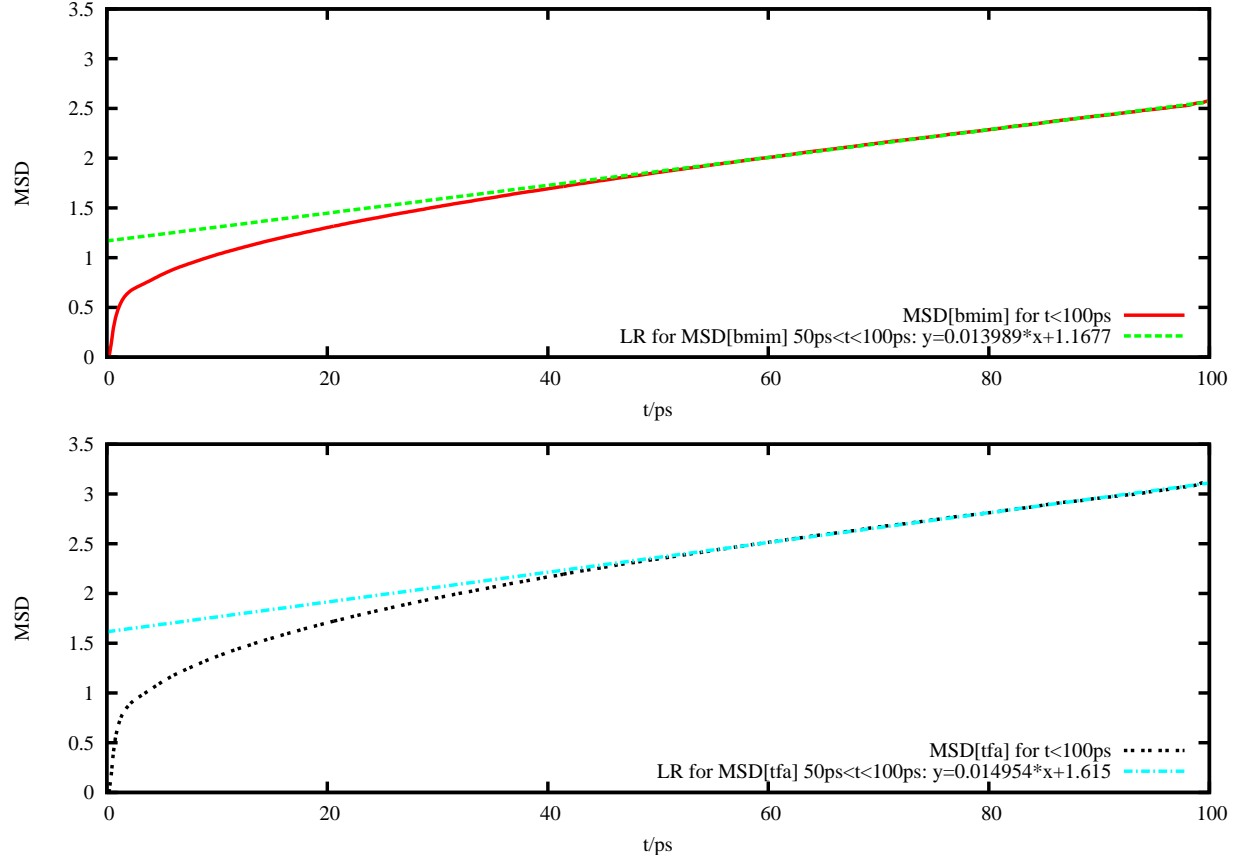TABLE IX: Diffusion coefficients $D/10^{-7}cm^2s^{-1}$.

FIG. 7: **[bmim][tfa]**: MSD ($\langle \Delta \mathbf{r}(t)^2 \rangle / \mathring{A}^2$) of the cation, [bmim], and the anion, [tfa]. The linear regression (LR) for the most linear part of the curve is given as well.

d.   [emim][cla]   Calculated diffusion coefficients are listed in table X. The MSD for 50ps of 99 50ps-trajectory slices and the MSD for 500ps and 1000ps of a single 1000ps-trajectory slice were calculated. The respective curves are plotted in figures 8 and 9. Msd_A was used for the MSD of the 50ps-trajectory slices and Msd_B for the MSD of the 1000ps-trajectory slice. The 50ps-MSD curves of the chloride ([cla]) in figure 8 nicely demonstrate the effect of averaging. The curve becomes smoother when the sample size is increased from 9 to 99 MSD curves and when the "Sliding Window" averaging method is used. Surprisingly, the gradient falls and the ordinate intercept rises considerably with increasing statistics. Nonetheless, these curves are much to short to use the gradient of their most linear part in the Einstein formula. The 500ps-MSD becomes linear after $t = 100ps$ until about $t = 350ps$ (figure 9) and the gradient of this part represents diffusion more reliable. Afterwards the "Sliding Window" averaging has almost no effect which can be seen by the ripples and the deviation from linearity. Therefore, these MSD-values can be neglected.

So far, few investigations on conductivity were reported for the system [emim][cla] which has some peculiarities: First, it has a relatively high melting point of about 78°Celsius and therefore had to be simulated at 400K. Second and third, it is the largest system for which the MSD was calculated and the MSD itself was calculated for the longest time interval (500ps). Therefore, the diffusion coefficient should be calculated from a larger sample to end up with reliable values.

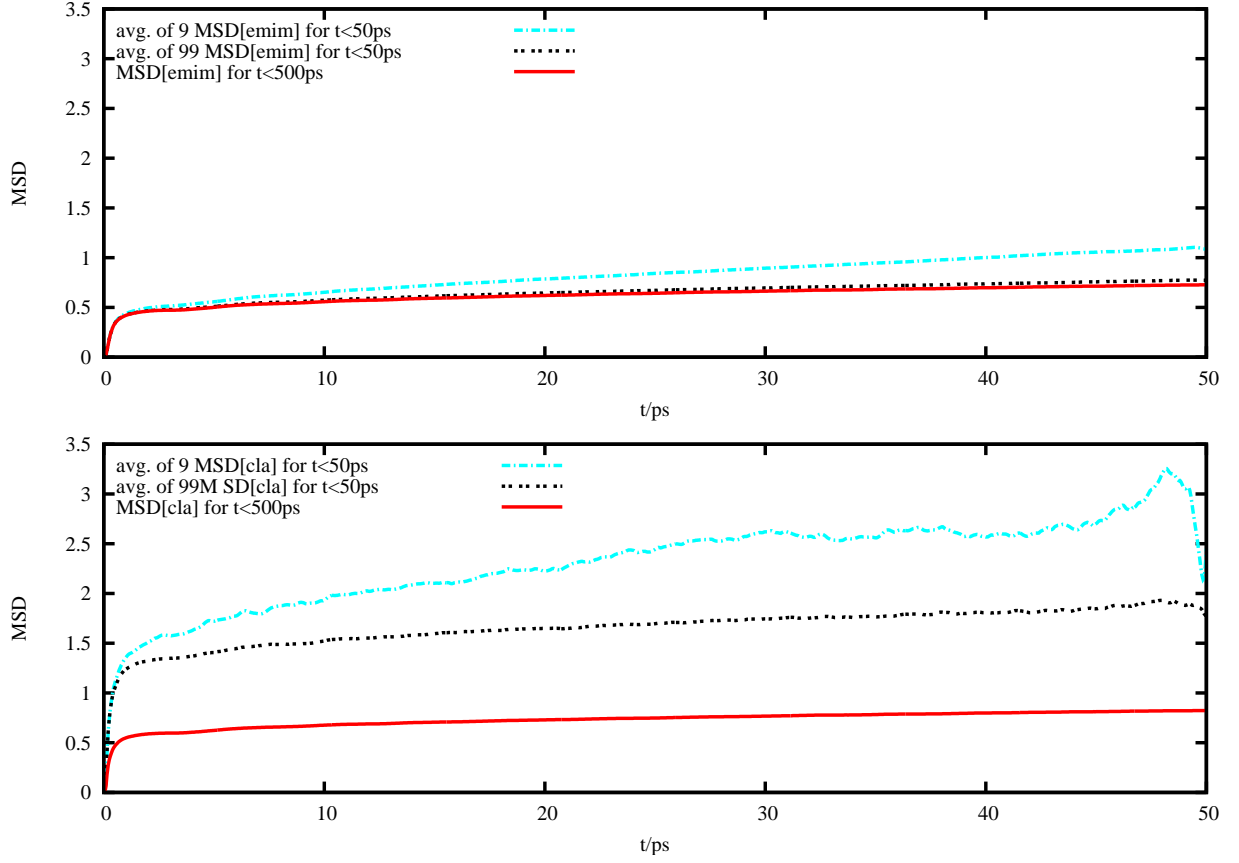| Ion	D_{500ps}
[emim]	0.20
[cla]	0.15

TABLE X: Diffusion coefficients $D/10^{-7}cm^2s^{-1}$.

FIG. 8: **[emim][cla]**: MSD ($\langle\Delta\mathbf{r}(t)^2\rangle/\mathring{A}^2$) of the cation, [emim], and the anion [cla] (below). The average 50ps-MSD of 9, and 99 50ps-trajectory slices, as well as a 50ps-MSD of a 1000ps-trajectory slice are depicted in both diagrams to show the effect of averaging.
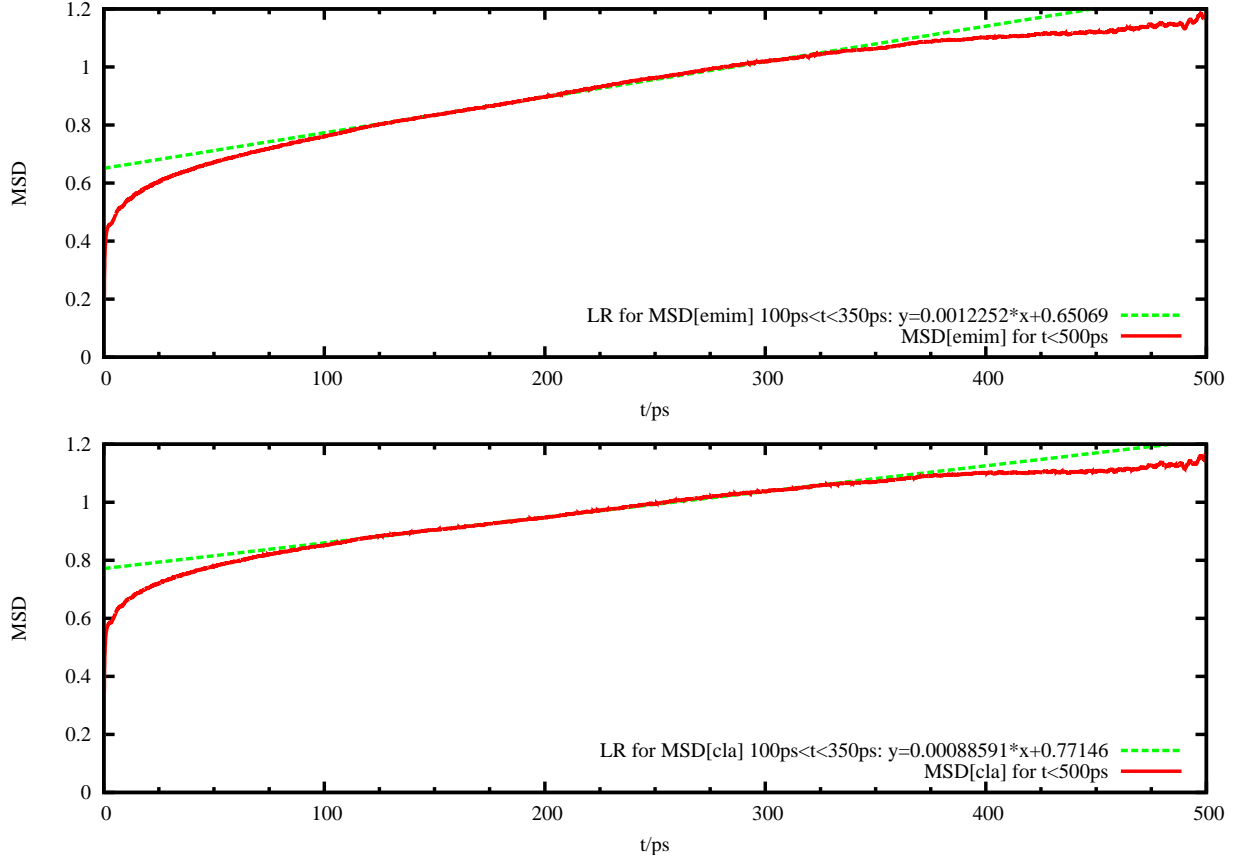
FIG. 9: **[emim][cla]**: MSD ($\langle\Delta\mathbf{r}(t)^2\rangle/\mathring{A}^2$) of the cation, [emim], and the anion [cla] (below), as well as their linear regressions lines (LR).

System	D_+	D_-	$D_{+,exp}$	$D_{-,exp}$	$D_{+,MD}$	$D_{-,MD}$
[bmim] [bf4]	1.31 *	1.26 *				
	0.94	0.61	1.598 [a]	1.492 [a]	0.18 [b]	0.17 [b]
[bmim] [pf6]	0.40	0.21	0.802 [a]	0.586 [a]	0.33 [b]	0.24 [b]
					0.970 [c]	0.882 [c]
[bmim] [tfa]	2.3	2.5	1.974 [a]	1.584 [a]		
[emim] [cla]	0.20	0.15			3.61 *[d]	1.43 *[d]

TABLE XI: Diffusion coefficients ($D/10^{-7} cm^2 s^{-1}$) for the investigated ILs. Values in columns D_+, and D_- are from this work and are calculated from MSD curves except values with the superscript "*" which are calculated from VACFs. Note that results for the system [emim][cla] are valid for T=400K. Diffusion coefficients from literature are also included in columns $D_{+,exp}$, and $D_{-,exp}$ for experimental results, and $D_{+,MD}$, and $D_{-,MD}$ for molecular dynamics simulation results: "a": Ref. 24, "b": Ref. 23, "c": Ref. 26, "d": Ref. 22.

To give an overview, the calculated diffusion coefficients are listed and compared to results from literature, both experimental and simulated, in table XI. For the systems [bmim][bf4], [bmim][pf6], and [bmim][tfa] the results are in a good agreement with literature although the length of the MSDs of this work are considerably shorter. On the other hand, the sample size from which the average MSD was calculated is higher: from 50 to 250 trajectory slices. The system [emim][cla] sticks out in that the 500ps-MSD is the average of two strongly differing 500ps-MSD curves, i.e. the calculated diffusion coefficient is based on insufficient statistics. Moreover, Vega et al. report diffusion coefficients almost 20 and 10 times larger for the cation and anion, respectively.

Finally, in figure 10 the first picosecond of various MSD functions are displayed for comparison. The MSD generally rises quickly, almost exponentially, for $t < 0.1$ to $0.2ps$ which is best seen in the MSD of chloride, [cla], in [emim][cla]. First, this reminds of the minimum of the VACF at about $0.3ps$ which has been attributed the mean collision time of a single particle. This fast process has been interpreted in Ref. 27 as the exploration of the local energy landscape by the particle. The nonlinear subsequent MSD, e.g. for $0.2ps < t < 0.4ps$ of [emim], has been interpreted as "energy basin hopping" of the particle. Finally, the curvature vanishes and the MSD becomes straight which has been attributed the diffusive linear behavior.

Additionally, figure 10 exhibits the effect of "coarse graining" in the time domain of the MSD. The length between successive MSD values varies among the systems from 0.02ps for [bmim][bf4] and [bmim][pf6], to 0.05ps for [emim][cla], up to 0.2ps for [bmim][tfa]. Except for the smoothness of the curve the MSD is faithfully reproduced with longer timesteps between successive MSD values.
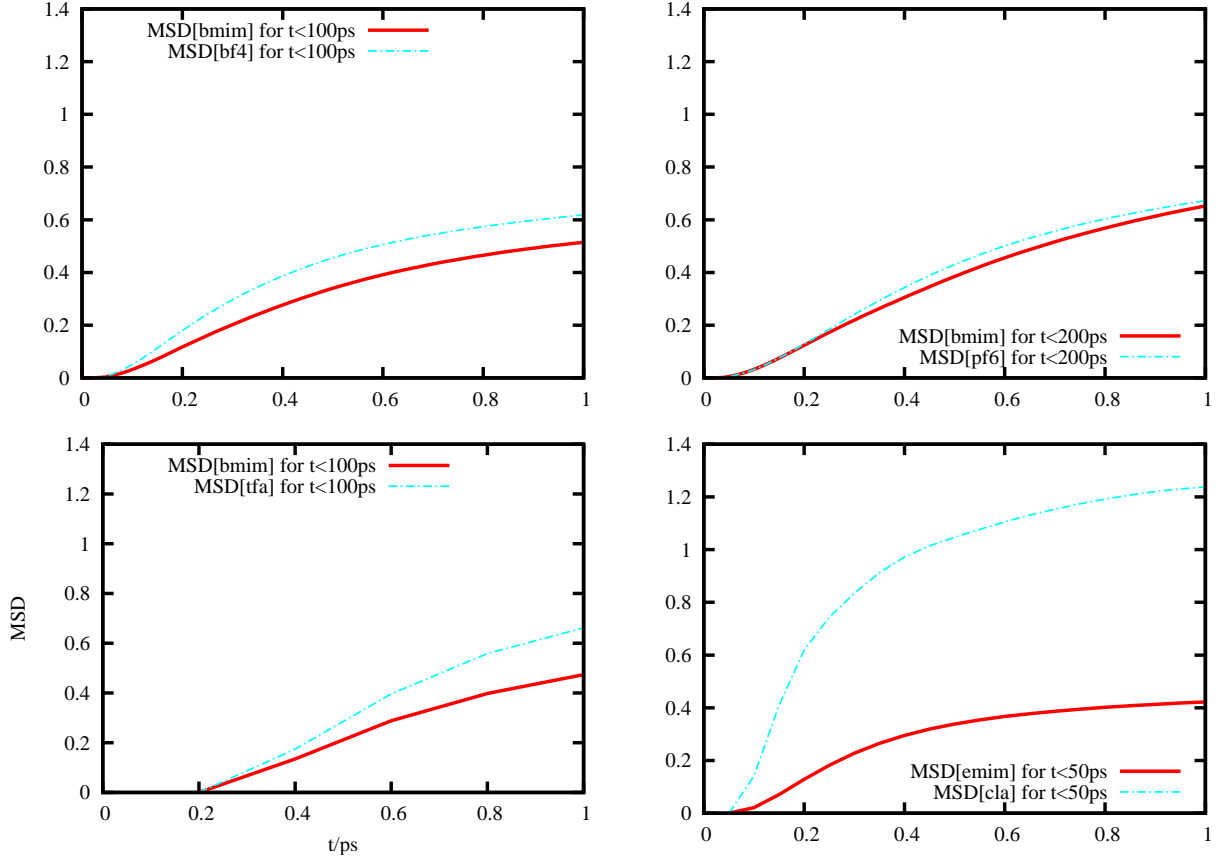
FIG. 10: Zoom-in on the first picosecond of the MSD ($\langle \Delta \mathbf{r}(t)^2 \rangle / \mathring{A}^2$ for $t < 50ps$) of [bmim][bf4], [bmim][pf6], [bmim][tfa], and [emim][cla].

B. Conductivity

1. Green-Kubo Formula: Current Auto-Correlation Function

The time-dependent collective current was determined with the program ADD_VELCM and then its auto-correlation function (CACF) with the program CORREL_VELCM. The resulting correlation function, being a collective property correlation function, revealed a very high noise (figure 11) and had to be refined using the "Running Average" algorithm (RAVG)(figure 12). The "Savitzky-Golay" filter as well as a "High-Pass" and a "Low-Pass" filter didn't prove as effective for refinement, as judged by visual inspection (data not shown). Obviously, the integral of the CACF converges after a couple of picoseconds and subsequently fluctuates strongly around a mean value. The worsening statistics towards the end of the CACF and its integral are present as in the VACF. It is expected that the CACF - being a collective property auto-correlation function - decays faster than the VACF. To be sure, the value of the integral was averaged between 1000ps and 7000ps with the program PERLSTAT for the integrals of the normal and RAVG-refined CACFs before calculating the conductivity (table IV B 1).

The results are in excellent agreement with the experimental findings of Yamamoto et al.[28] and Watanabe et al.[24]. As already mentioned, the Nernst-Einstein relation (sections IV A 1 and IV A 2) overestimates the conductivity, in this case by a factor $\sigma_{NE}/\sigma_{GK} = 4.785/3.17 = 1.5$. In contrast, the Einstein-Helfand relation yields different results (section IV B 2).

Figure 13 gives a detailed picture of the first 10ps of the CACF and figure 14 of both the CACF and its integral. The higher noise as compared to the VACF and its integral is evident.

Refinement	Integral of CACF $/\mathring{A}^2 e^2 AKMA^{-2}ps$	$\sigma_{GK}/10^{-3}Scm^{-1}$
none	0.001 ± 0.001	2.37
RAVG30	$0.00128 \pm 5.7 \cdot 10^{-5}$	3.17
RAVG50	$0.00124 \pm 3.3 \cdot 10^{-5}$	3.06
RAVG70	$0.00131 \pm 2.6 \cdot 10^{-5}$	3.23

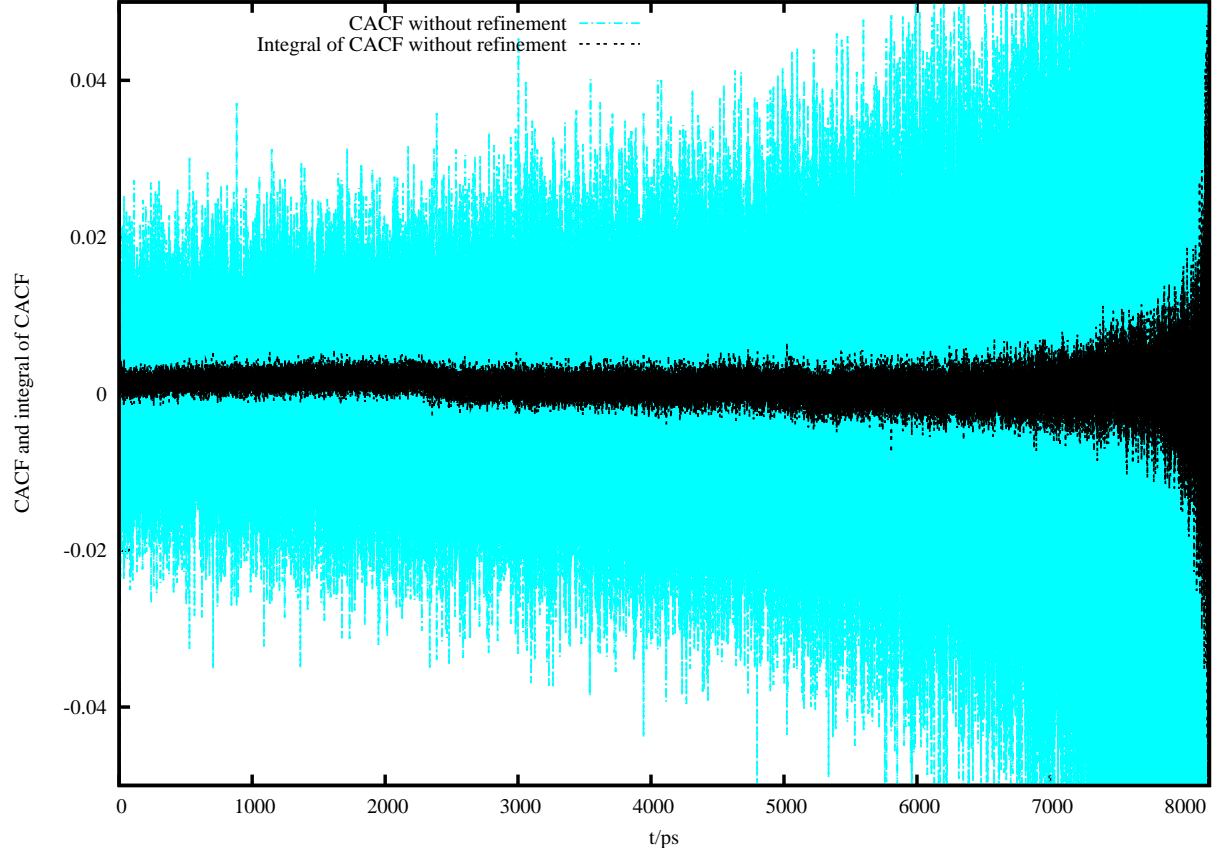TABLE XII: Averages of the integral of the CACF and conductivities.

53

FIG. 11: **[bmim][bf4]**: The CACF ($\langle J(0)J(t)\rangle/e^2\mathring{A}^2AKMA^{-2}$) and its integral ($\int\langle J(0)J(t)\rangle\mathrm{d}t/e^2\mathring{A}^2AKMA^{-2}ps$) without any refinement.
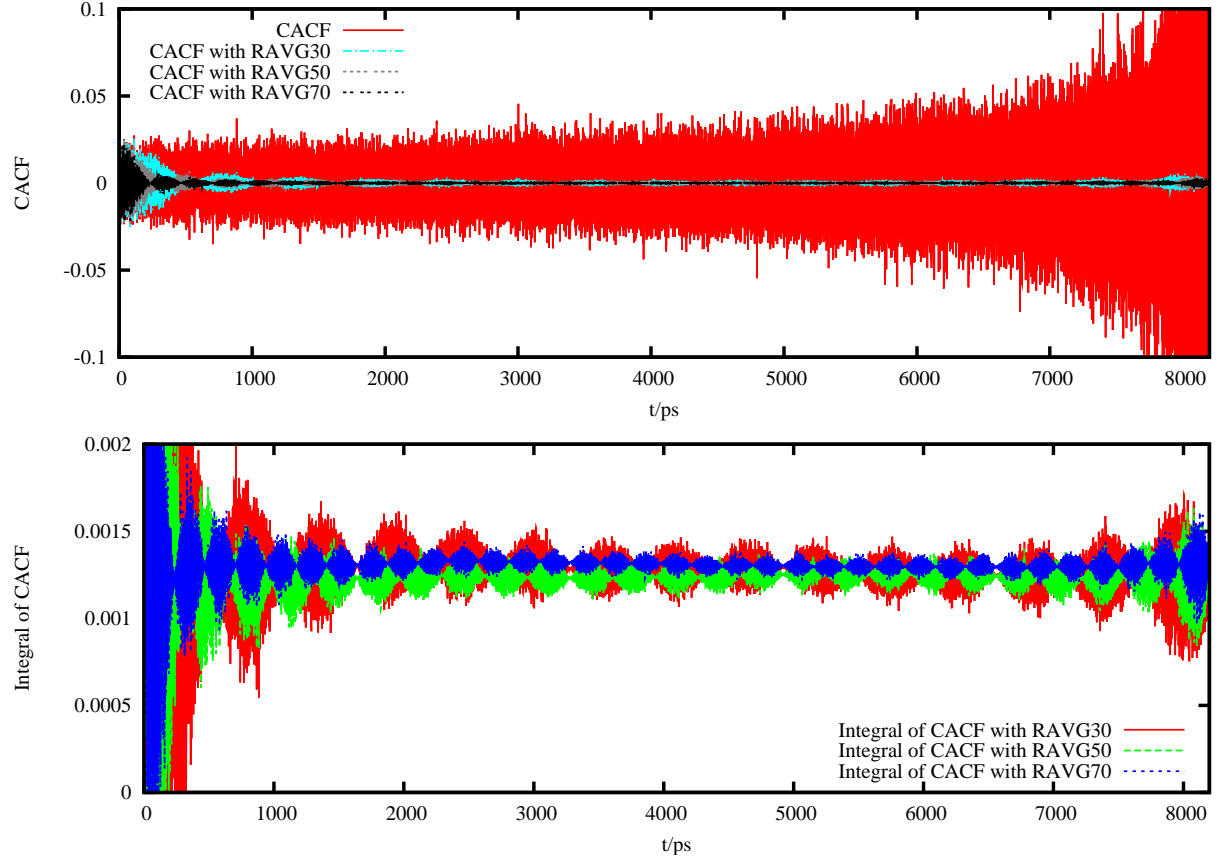
FIG. 12: [**bmim**][**bf4**] The CACF ($\langle J(0)J(t)\rangle/e^2 \mathring{A}^2 AKMA^{-2}$) averaged with "Running Average" using 30, 50, and 70 points (above) and their respective integrals ($\int \langle J(0)J(t)\rangle \mathrm{d}t/e^2 \mathring{A}^2 AKMA^{-2} ps$) (below).
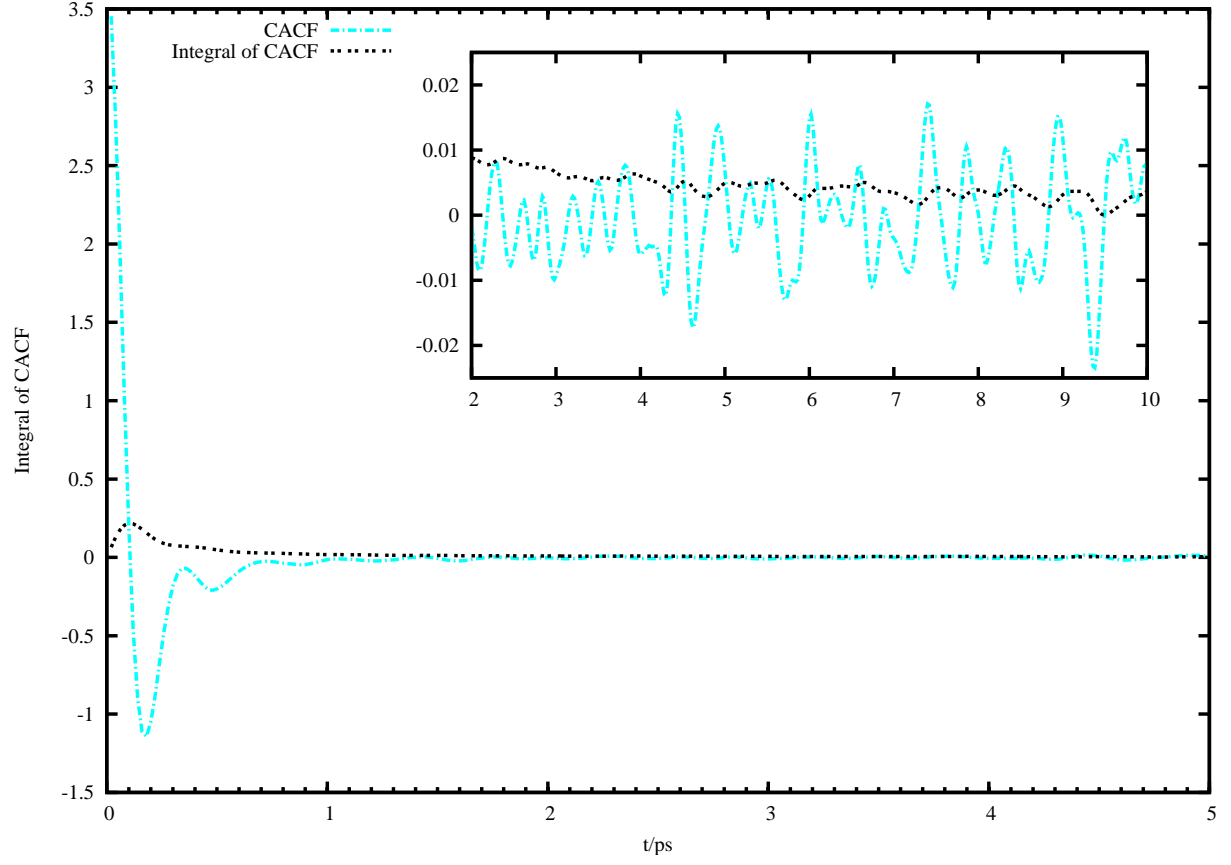
FIG. 13: [**bmim**][**bf4**]: The first 5ps of the CACF ($\langle J(0)J(t)\rangle/e^2 \mathring{A}^2 AKMA^{-2}$) and its integral ($\int \langle J(0)J(t)\rangle \mathrm{d}t/e^2 \mathring{A}^2 AKMA^{-2}ps$) and a zoom-in on subsequent 5ps.
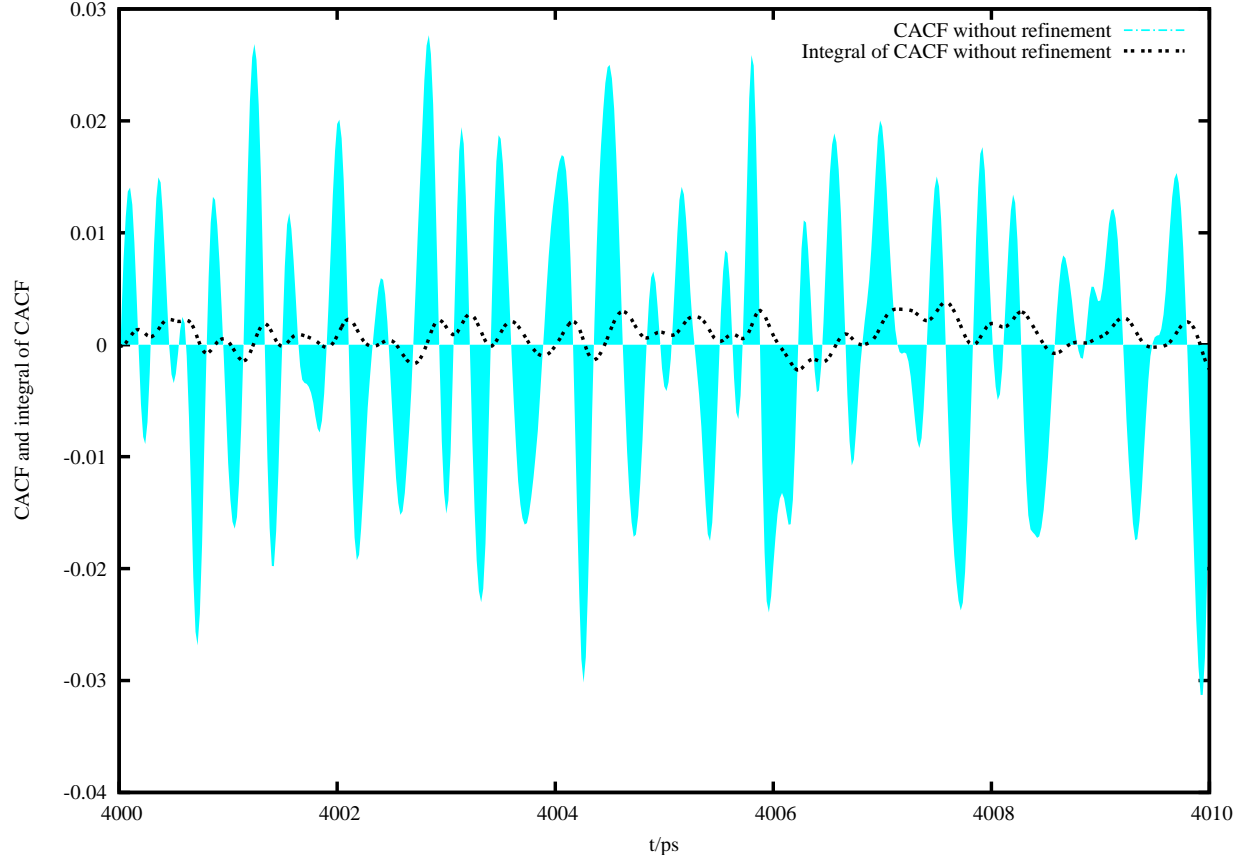
FIG. 14: **[bmim][bf4]**: The CACF $(\langle J(0)J(t)\rangle/e^2\mathring{A}^2AKMA^{-2})$ and its integral $(\int\langle J(0)J(t)\rangle \mathrm{d}t/e^2\mathring{A}^2AKMA^{-2}ps)$ for the segment 4000ps to 4010ps. The area beneath the auto-correlation function is filled to depict the its and its integral's fluctuations.

2. Einstein-Helfand Formula: Mean Square Displacement of the Translational Dipole Moment

The mean square displacement of the translational dipole moment, i.e. $\langle \Delta \mathbf{M}_J(t)^2 \rangle$, or MSDMJ in short, was calculated with the program MJMJ for the systems [bmim][bf4], [bmim][pf6], [bmim][tfa], [emim][cla], [emim][dcyi], [emim][trif] and [evot][dcyi]. The conductivity, as expressed in the Einstein-Helfand formula is proportional to the gradient of the MSDMJ which is deduced by linear regression (LR). The LR curves are mostly included in the diagrams to highlight the linear part of the MSDMJ curves.

a. [bmim][bf4] Figure 15 shows the MSDMJ for 100ps of a 100ps-trajectory slice. The noise stays high throughout the whole time. Consequently, the MSDMJ was calculated for a shorter time interval (40ps) and averaged over 140 100ps slices which brought about better statistics by "Sliding Window" averaging and thus a smoother curve which could be subjected to linear regression in the linear part to extract the slope (results are given in tables XIII and XX).

This outcome is in perfect agreement with results in sections IV A 1, IV A 2, and IV B 2 but it is almost sure that the linear part of the MSDMJ curve hasn't begun within 40ps as exemplified in figure 15. Calculating the LR of the average MSDMJ for 1000ps from 9 4000ps-trajectory slices revealed a substantially differing slope.

Considering that the calculated viscosity from the very same simulation data was over-rated by about 60 %[19] and assuming that Walden's rule ($\sigma\eta = const$) roughly applies a conductivity reduced by a factor $1/1.6 = 0.625$ would be expected. The calculated value is even reduced by a factor $\sigma_{EH}/\sigma_{GK} = 0.76/3.17 \approx 0.24$.

# of trajectory slice	Length of trajectory slice	Length of MSDMJ	σ_{EH}
140	100ps	40ps	3.64
9	4000ps	1000ps	0.76

TABLE XIII: **[bmim][bf4]**: Conductivities ($\sigma_{EH}/10^{-3}Scm^{-1}$) from MSDMJ functions of different lengths: 40ps and 1000ps.
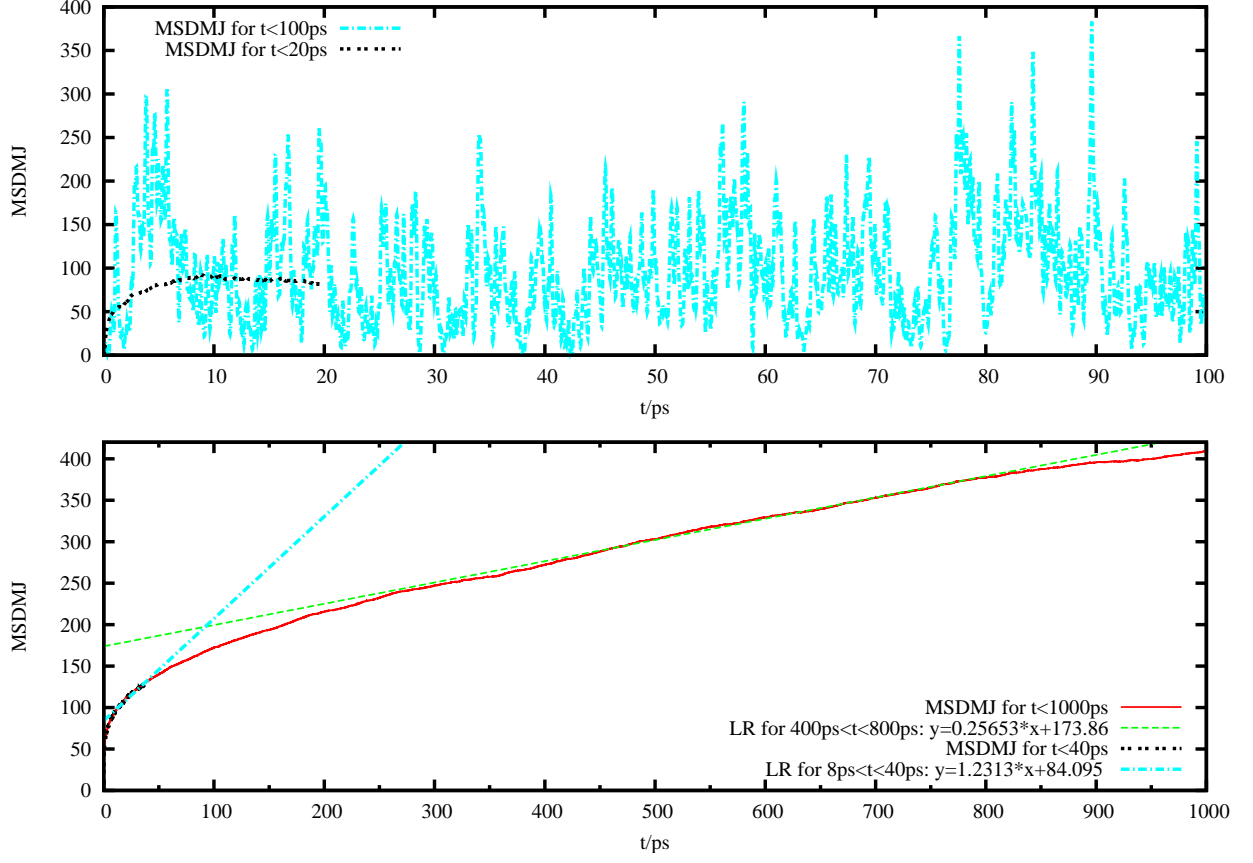
FIG. 15: **[bmim][bf4]**: The upper diagram demonstrates the noise in MSDMJ ($\langle \Delta \mathbf{M}_J(t)^2 \rangle / e^2 \mathring{A}^2$) of [bmim][bf4] with (short MSDMJ curve) or without (long MSDMJ curve) "Sliding Window" averaging. The diagram below depicts the 40ps-MSDMJ and the 1000ps-MSDMJ together with their LR curves.

b. [bmim][pf6] Figure 16 contains the results of the MSDMJ analysis, the averaged 200ps-MSDMJ of 50 200ps-trajectory slices. Despite the high noise a trend is perceptible which allows to estimate a slope and conductivity. The second illustrates the 40ps-MSDMJ of the same sample which is smoother due to "Sliding Window" averaging but with a steeper gradient.

As for [bmim][bf4], the 40ps-MSDMJ has not reached a plateau and is too short. The resulting values are listed in tables XIV and XX. The conductivity from the 200ps-MSDMJ is in perfect agreement with estimates from the Nernst-Einstein relation which overrates by a factor $\sigma_{NE}/\sigma_{EH} = 0.72/0.54 = 1.3$ and calculations by Kolafa et al.[23].

# of trajectory slice	Length of trajectory slice	Length of MSDMJ	σ_{EH}
50	200ps	200ps	0.54
50	200ps	40ps	1.53

TABLE XIV: **[bmim][pf6]**: Conductivities ($\sigma_{EH}/10^{-3}Scm^{-1}$) from MSDMJ functions of different lengths: 40ps and 200ps.
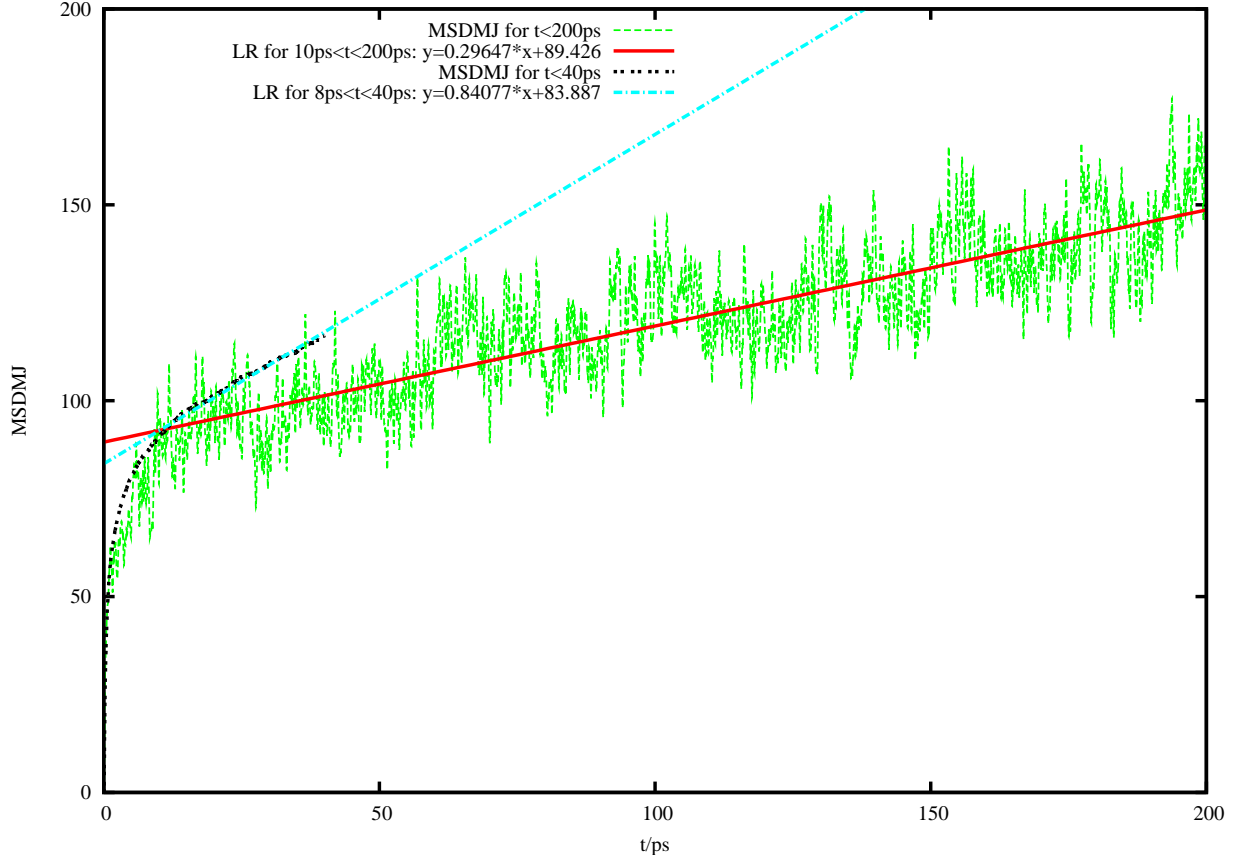
FIG. 16: [**bmim**][**pf6**]: The noise in MSDMJ ($\langle \Delta \mathbf{M}_J(t)^2 \rangle / e^2 \mathring{A}^2$) for 200ps compared to 40ps and corresponding LR curves.

c. *[bmim][tfa]* Figure 17 shows the 40ps-MSDMJ of 250 100ps-trajectory slices, the 250ps-MSDMJ of a single 4000ps-trajectory slice and the averaged 1000ps-MSDMJ of three 4000ps-trajectory slices with slopes and corresponding conductivities given in tables XV and XX.

The 40ps-MSDMJ has to be neglected. The results for the other MSDMJ curves are in rough accordance with literature and even rougher with estimates from the Nernst-Einstein relation which overrates in this case by a factor $\sigma_{NE}/\sigma_{EH} = 8.1/4.1 = 2$ and $8.1/2.6 = 3.1$.

# of trajectory slice	Length of trajectory slice	Length of MSDMJ	σ_{EH}
250	100ps	40ps	6.64
1	4000ps	250ps	4.11
3	4000ps	1000ps	2.81

TABLE XV: **[bmim][tfa]**: Conductivities ($\sigma_{EH}/10^{-3}Scm^{-1}$) from MSDMJ curves of different lengths: 40ps, 250ps, and 1000ps.
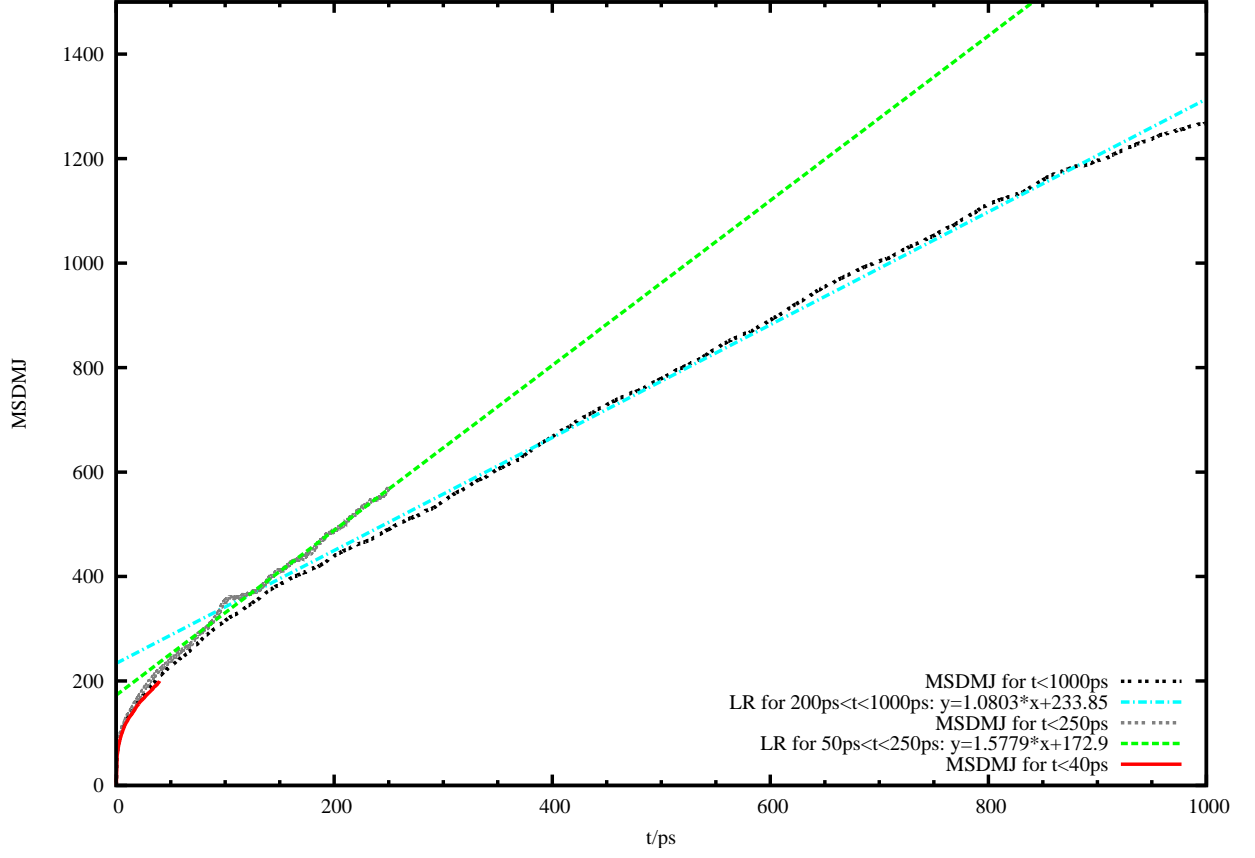
FIG. 17: [**bmim**][**tfa**]: MSDMJ ($\langle \Delta \mathbf{M}_J(t)^2 \rangle / e^2 \mathring{A}^2$) and LRs for 40ps, 250ps, and 1000ps.

d. *[emim][cla]* The 40ps-MSDMJ was calculated from 599 50ps-trajectory slices, and 9 2000ps-trajectory slices were evaluated to extract 250ps-, the 500ps-, and the 1000ps-MSDMJ curves (see figure 18 and tables XVI and XX). A 2000ps-MSDMJ proved too noisy for interpretation.

Again, the 50ps-MSDMJ has to be neglected. Though in accordance with estimates from the Nernst-Einstein relation $\sigma_{NE}/\sigma_{EH} = 0.6/0.3 = 2$ the conductivities from 500ps- and 1000ps-MSDMJ are lower than reported in literature[22] by a factor 20, just as the diffusion coefficients IV A 2.

# of trajectory slice	Length of trajectory slice	Length of MSDMJ	σ_{EH}
599	50ps	40ps	1.43
9	2000ps	500ps	0.32
9	2000ps	1000ps	0.30

TABLE XVI: **[emim][cla]**: Conductivities ($\sigma_{EH}/10^{-3}Scm^{-1}$) from MSDMJ functions of different lengths: 40ps, 250ps, and 1000ps.
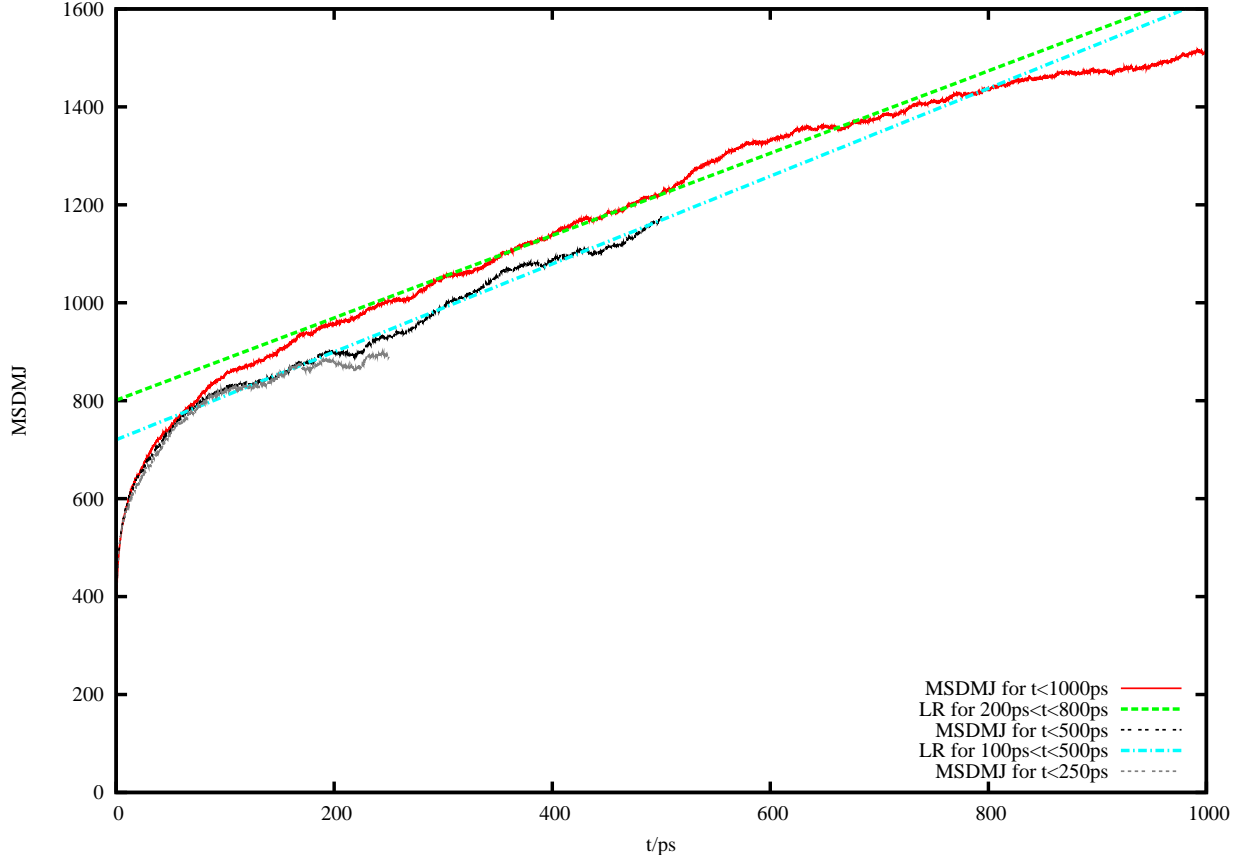
FIG. 18: [**emim**][**cla**]: MSDMJ ($\langle \Delta \mathbf{M}_J(t)^2 \rangle / e^2 \AA^2$) and LRs of 40ps, 500ps, and 1000ps.

e.   [emim][trif]   Here, the effect of the "Sliding Window"-averaging was thouroughly tested. MSDMJ curves from a 2000ps-trajectory slice were calculated for different lengths (200ps, 199ps, 195ps, 190ps, 175ps, 150ps, and 100ps) to follow the smoothening of the curves with increasing statistics (cf. figure 19). The 50ps-MSDMJ was also determined for 250 50ps-trajectory slices as well as from 3 200ps-trajectory slices which is depicted in figure 19. The corresponding results are listed in tables XVIII and XX.

The 50ps-MSDMJ has to be neglected. As for the 100ps-MSDMJ, no comparisons can be drawn to Nernst-Einstein estimates and a single reference reports a conductivity 8.4 times as high[29]. The statistics of the corresponding MSDMJ curve is the lowest among the systems in this work and therefore the calculated conductivity is not reliable.

# of trajectory slice	Length of trajectory slice	Length of MSDMJ	σ_{EH}
250	50ps	50ps	1.62
3	200ps	50ps	1.62
1	200ps	100ps	1.1

TABLE XVII: [**emim**][**trif**]: Conductivities ($\sigma_{EH}/10^{-3} Scm^{-1}$) from MSDMJ functions of different lengths.
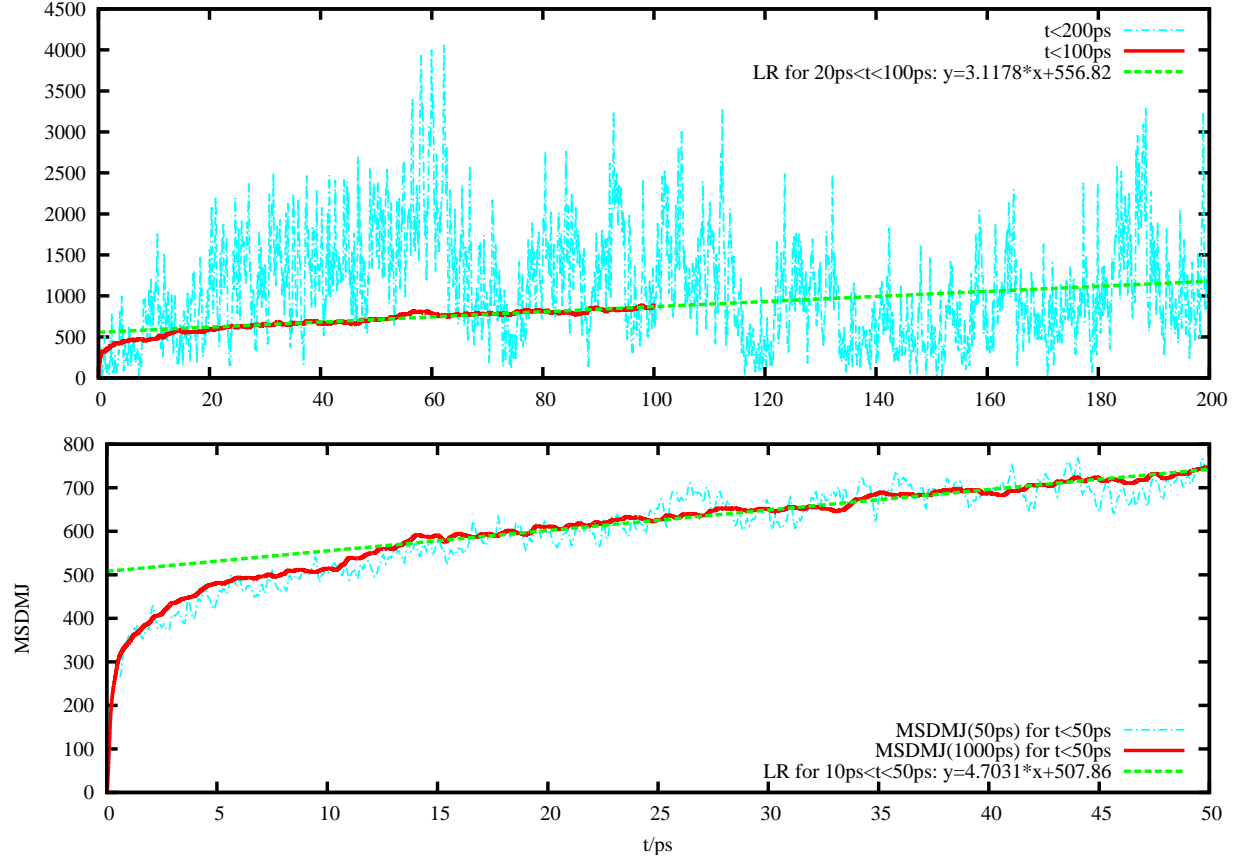
FIG. 19: **[emim][trif]**: MSDMJ ($\langle\Delta\mathbf{M}_J(t)^2\rangle/e^2\mathring{A}^2$) for 100ps and 200ps (above) and for 50ps (below).

f. [emim][dcyi] 500 40ps-MSDMJ curves were calculated from 200ps-trajectory slices and averaged, as well as a 1000ps-MSDMJ curve from 5 2000ps-trajectory slices which has quite an interesting shape with two different linear parts. The curves and values are listed in tables XVIII and XX and figure 20.

The 40ps-MSDMJ has to be neglected. The first linear part of the 1000ps-MSDMJ results in a conductivity slightly above the experimentally determined one whereas the second linear part is almost 1.5 times as steep.

# of trajectory slice	Length of trajectory slice	Length of MSDMJ	σ_{EH}
500	200ps	40ps	6.67
5	2000ps	1000ps	3.6 and 5.54

TABLE XVIII: [**emim**][**dcyi**]: Conductivities ($\sigma_{EH}/10^{-3}Scm^{-1}$) from the LRs of the linear parts of the MSDMJ functions.
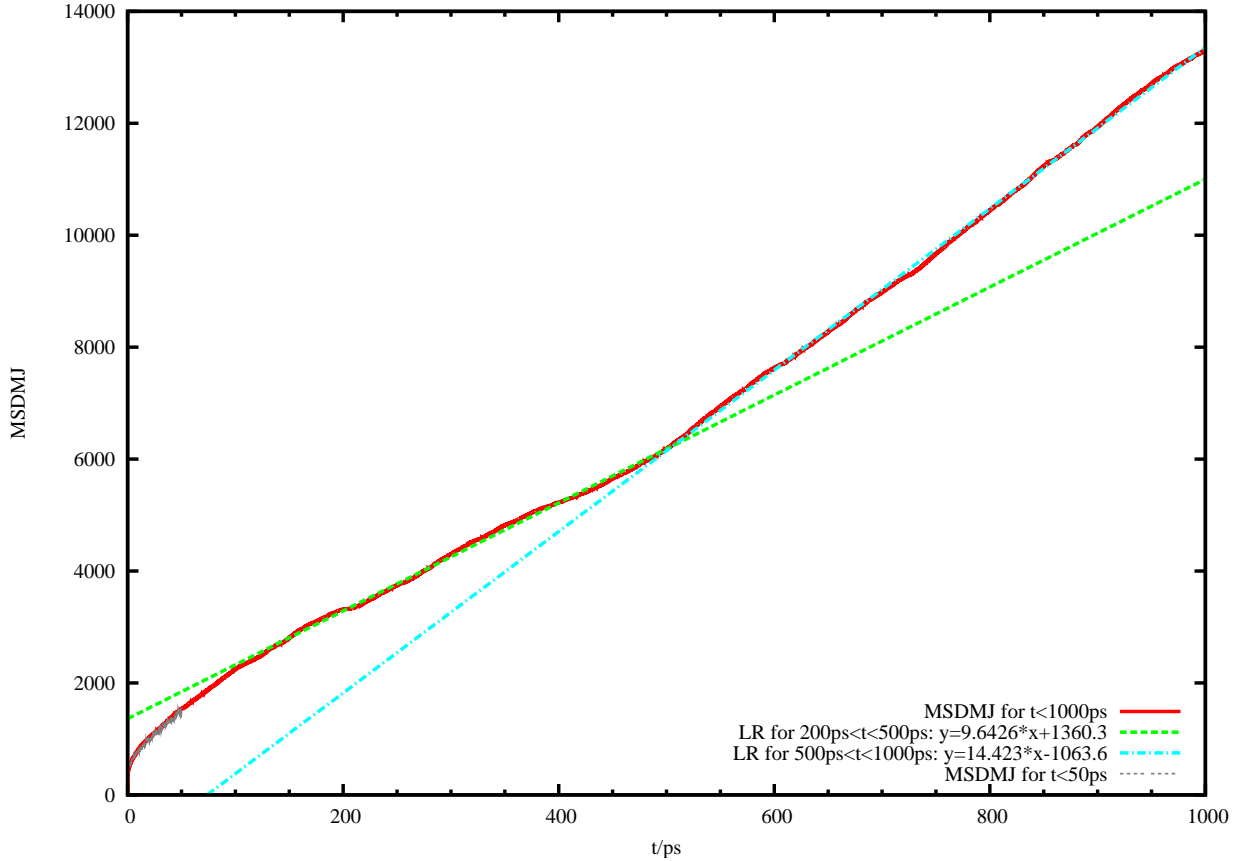
FIG. 20: [**emim**][**dcyi**]: $\langle \Delta \mathbf{M}_J(t)^2 \rangle / e^2 \mathring{A}^2$ of [emim][dcyi]

g.   [evot][dcyi]   This ion pair is the same as [emim][dcyi] but simulated with a different charge distribution[21]. 4 1000ps-trajectory slices were analyzed to yield a mean 500ps-MSDMJ which was further evaluated. The results are given in table XIX and figure 21. The gradient is close to the first linear part of the 1000ps-MSDMJ of [emim][dcyi].

# of trajectory slice	Length of trajectory slice	Length of MSDMJ	σ_{EH}
4	1000ps	500ps	3.86

TABLE XIX: **[evot][dcyi]**: Conductivities ($\sigma_{EH}/10^{-3}Scm^{-1}$) from the LRs of the linear parts of the MSDMJ functions.
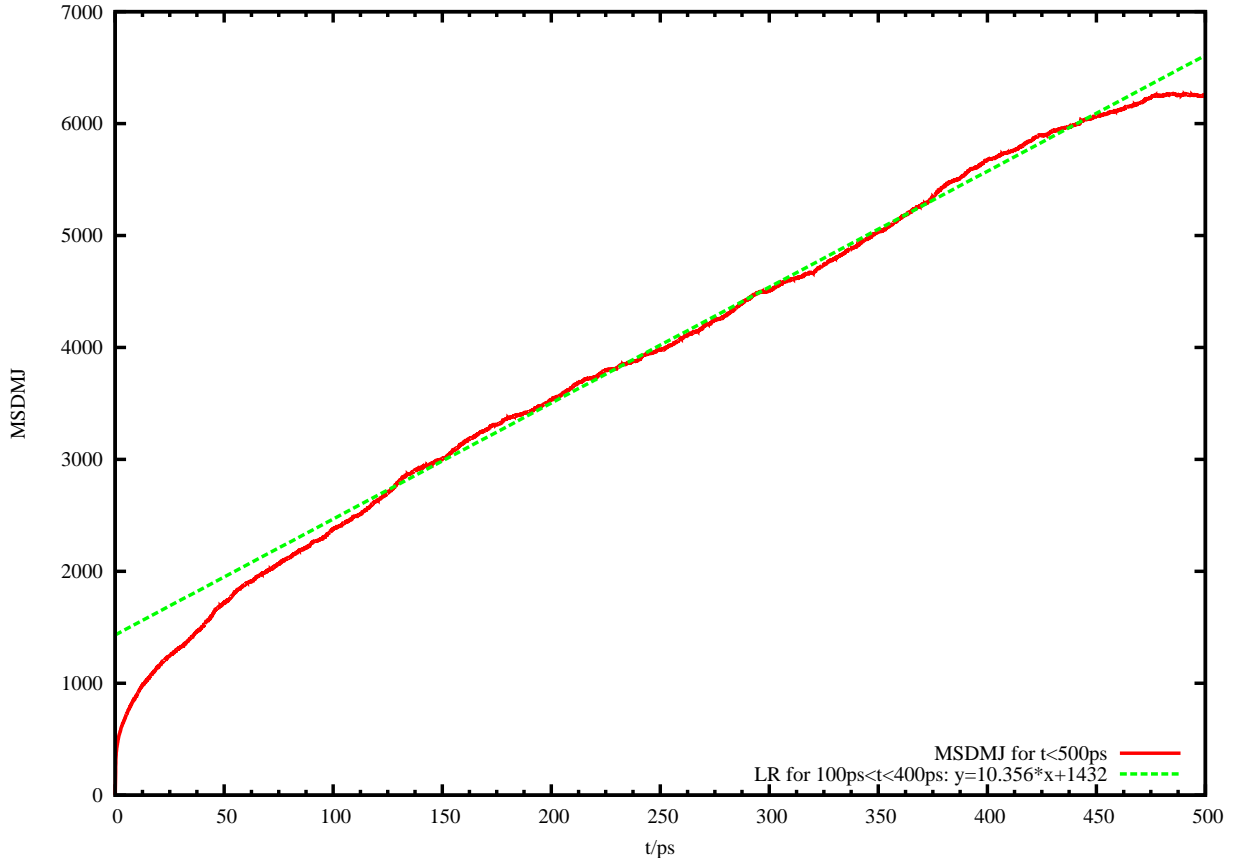

FIG. 21: **[evot][dcyi]**: $\langle \Delta \mathbf{M}_J(t)^2 \rangle / e^2 \mathring{A}^2$ of [evot][dcyi]

As for the MSD, the first picosecond of MSDMJ is presented in detail (figure 22). Here as well, the time domain of the MSDMJ was "coarse grained" and the time between successive steps of the MSDMJ evaluation was 0.001ps for [emim][trif], 0.02ps for the systems [bmim][bf4] and [bmim][pf6], and 0.05ps for [emim][dcyi]. Again the "coarse graining" had no effect on the overall course of the MSDMJ.
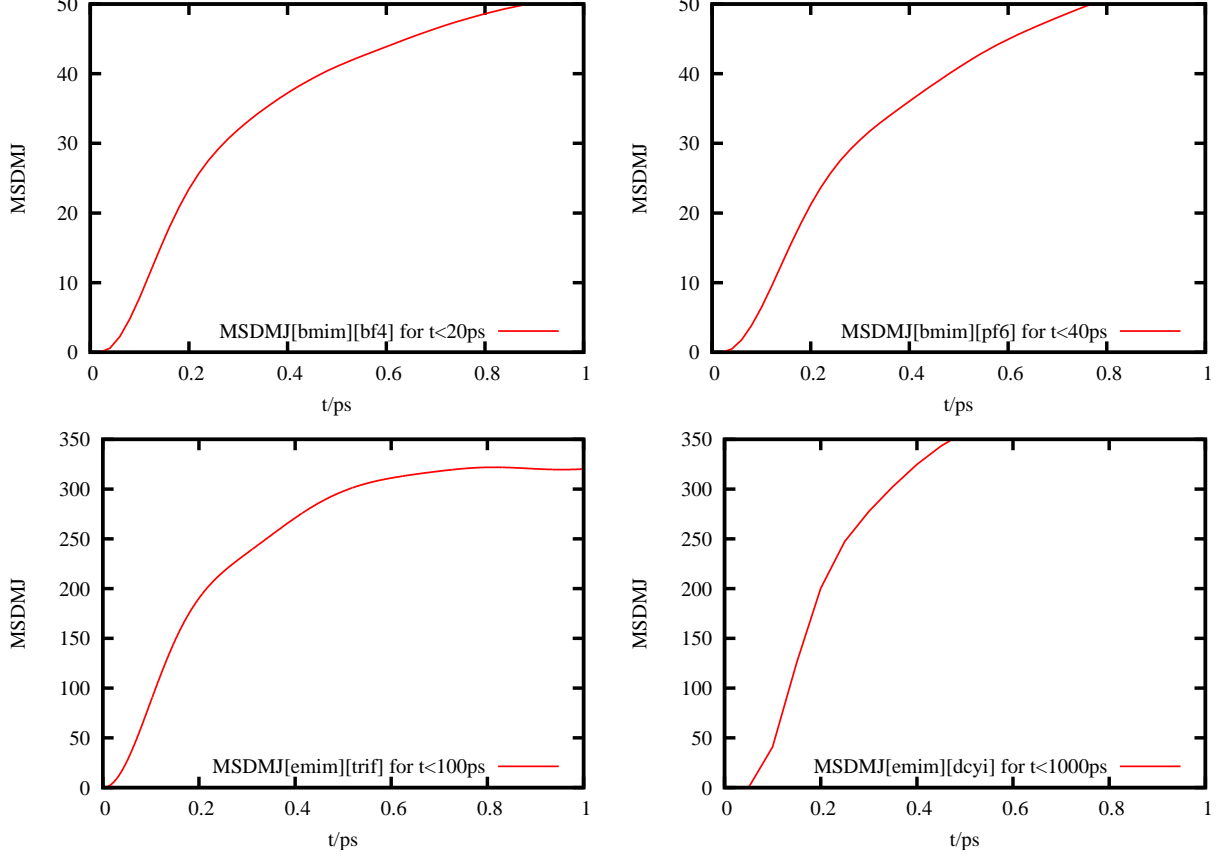

FIG. 22: $\langle \Delta \mathbf{M}_J(t)^2 \rangle / e^2 \mathring{A}^2$

70

System	σ_{NE}	σ_{EH}	σ_{exp}	σ_{MD}
[bmim] [bf4]	4.8 *	3.17 *	3.5 [a]	$\sigma_{EH} = 0.55$ [g]
	3.0	0.76	3.6 [b]	$\sigma_{NE} = 0.7$ [g]
[bmim] [pf6]	0.72	0.54	1.5 [b]	$\sigma_{EH} = 0.45$ [g] and 0.62 [g]
			1.46 [c]	$\sigma_{NE} = 1.05$ [g]
[bmim] [tfa]	8.1	4.11	3.1 [b]	
		2.81	3.2 [d]	
[emim] [cla]	0.6	0.32		$\sigma_{GK} = 7.2$ [h]
		0.30		$\sigma_{NE} = 9.2$ [h]
[emim] [trif]		1.1	9.2 [e]	
[emim] [dcyi]		3.6	2.8 [f]	
		5.4		
[evot] [dcyi]		3.86		

TABLE XX: Conductivities ($\sigma/10^{-3} Scm^{-1}$) for the investigated ILs. Values in columns σ_{NE} and σ_{EH} are from this work and are calculated from the Nernst-Einstein and Einstein-Helfand formulas, respectively. Values superscripted with "*" are obtained from the Green-Kubo formulas for VACFs and CACFs. The system [emim][cla] was simulated at T=400K. Conductivities values from literature are also included in columns σ_{exp} for experimental results, and σ_{MD} for molecular dynamics simulation results: "a": Ref. 28, "b": Ref. 30, "c": Ref. 31, "d": Ref. 32, "e": Ref. 29, "f": Ref. 33, "g": Ref. 23, "h": Ref. 22. Experimental results are obtained at T=298.1K.

V. CONCLUSION

In this work different ways to calculate the static conductivity of ILs were tested: first, the Green-Kubo formula, second, the Einstein-Helfand formula, and third, the Nernst-Einstein relation for estimating the conductivity by means of the diffusion coefficient which itself can be calculated by a Green-Kubo formula or an Einstein formula. The theoretical framework being straightforward the task was to implement them for trajectory data generated by CHARMM in a way that ensured both accuracy and efficiency. The used exact formulas are based on mean values of the whole sample, i.e. the whole phase space. To approximate these values reasonably well relatively large amounts of trajectory data, up to tens of nanoseconds, had to be analyzed. In contrast, to increase efficiency cuts on the analysis side had to be made. The outcome of this compromise is summarized and compared to results of literature in tables XI and XX.

All the diffusion coefficients are in qualitative agreement with findings from literature except for [emim][cla]. The VACF and 400ps-MSD of [bmim][bf4] and the 100ps-MSD of [bmim][tfa] accurately reproduce the experimental values. The 200ps-MSD of [bmim][pf6] deviates by a factor 2.

It turns out that MSD curves of at least 500ps length should be used to calculate diffusion coefficients. This minimum length ensures that the linear part of the MSD of which the gradient is proportional to the diffusion coefficient is included. Moreover, these curves should be well averaged over tens of non-overlapping trajectory slices since single MSD curves - though free from high noise - can have broadly varying gradients. Finally, the time between successive points of the MSD can be extended at least up to 0.2ps without losing any of the required accuracy.

As for the VACF, a 8.2ns trajectory slice allows to estimate a diffusion coefficient with a mean error of about 10% which is probably not in relation with the effort of generating a trajectory slice that long.

The conductivities are as well within an acceptable range of results of experiments and computer simulations from other groups. Computed from collective properties the most imminent issue is sufficient statistic averaging where the CACF is an outstanding example which could be controlled by the "running average" algorithm. Calculated from single particle variables and estimated by the Nernst-Einstein relation the conductivities are always

overrated by a factor 1.5 to 3.1 due to disregard of cross-correlation between different particles. The refined CACF of [bmim][bf4] evaluates to a conductivity which meets the experimentally measured value very well. This afforded a 8.2ns trajectory. The 1000ps-MSDMJ curve of [bmim][tfa] also scores within 10% of experimental values. The conductivities from [bmim][pf6] deviate by a factor 2 and from [emim][cla], and [emim][trif] by more than a factor 10. The latter MSDMJ calculations evidently need to be based on higher statistics, i.e. a larger sample of trajectory slices.

Just as for the MSD curves, firstly, it is seems to be necessary to calculate at least 500ps of the MSDMJ to comprise a sufficiently long part of the linear rise. Secondly, the 500ps-MSDMJ should be averaged over tens of non-overlapping trajectory slices. Finally, also the time between successive MSDMJ steps can be extended at least up to 0.2ps without cutbacks on the accuracy.

It is still necessary to fill the gaps in the samples of MSD and MSDMJ curves to obtain more reliable results. Furthermore, a systematic analysis of the mentioned potential economizations could show their limits clearlier.

Finally, it should be added that CHARMM determines the diffusion coefficient from the MSD by invoking a subroutine which computes correlation functions which is exact. Thereby, CHARMM optimizes the calculation. The reason why CHARMM was not used for this work lies in the fact that it was not possible to calculate the MSD of the center of mass position vector of a molecule which excludes any rotational movement irrelevant to diffusion. A program implementing both a CHARMM-like optimized algorithm and the center of mass position vector is on the way.

VI. APPENDIX

A. Abbreviations

VACF	$\langle \mathbf{v}(0)\mathbf{v}(t)\rangle / \mathring{A}^2 AKMA^{-2}$
VACF Integral	$\int \langle \mathbf{v}(0)\mathbf{v}(t)\rangle \mathrm{d}t / \mathring{A}^2 AKMA^{-2}ps$
CACF	$\langle J(0)J(t)\rangle / e^2 \mathring{A}^2 AKMA^{-2}$
CACF Integral	$\int \langle J(0)J(t)\rangle \mathrm{d}t / e^2 \mathring{A}^2 AKMA^{-2}ps$
MSD	$\langle \Delta\mathbf{r}(t)^2\rangle / \mathring{A}^2$
MSDMJ	$\langle \Delta\mathbf{M}_J(t)^2\rangle / e^2 \mathring{A}^2$
RAVG	Running Average (see section III C)

B. Units

$AKMA$ is the internal time-unit of CHARMM. $1AKMA = 0.04888ps$ or $20AKMA \approx 1ps$

C. Auxiliary calculations for the GK-diffusion coefficients in Phython

Conversion of the integral of the VACF to the diffusion coefficient in SI-units and calculation and calculation of the conductivity according to the Nernst-Einstein relation:

```
>>> 1./3*1e-8**2*0.04888**(-2)*1e12*9.4e-6
1.3114272525074489e-07
>>> 1./3*1e-8**2*0.04888**(-2)*1e12*8.8e-6
1.2277191300069736e-07


>>> 1./(1.380568e-23*300*(32.7*1e-8)**3)*1.60217733e-19**2*(108*1.3e-7+108*1.2e-7)
0.0047858889097789434
```

D. Auxiliary calculations for the MSD-diffusion coefficients and the NE-conductivities in Phython

```
>>> 0.0056358/6
0.00093930000000000001
>>> 0.0036668/6
0.0006111333333333333
>>> 1./(1.380658e-23*300*(32.7*1e-8)**3)*1.60217733e-19**2*(108*0.0009393e-4+108*0.00061113e-4)
0.0029678871999142919
```

74

```
>>> 0.0024066/6
0.00040109999999999999
>>> 0.0012666/6
0.00021110000000000001
>>> 1./(1.380658e-23*300*(38.4*1e-8)**3)*1.60217733e-19**2*(108*0.40110e-7+108*0.21110e-7)
0.0007236643926502533

>>> 0.013989/6
0.0023314999999999998
>>> 0.014954/6
0.0024923333333333334
>>> 1./(1.380658e-23*300*(34.1*1e-8)**3)*1.60217733e-19**2*(108*0.013989e-4+108*0.014954e-4)/6
0.0081426676512256196

>>> 0.0012252/6
0.0002042
>>> 0.00088591/6
0.00014765166666666667
>>> 1./(1.380658e-23*400*(60.13*1e-8)**3)*1.60217733e-19**2*(1000*0.0022167e-4+1000*0.0020738e-4)/6
0.0015288261556470719
```

E.   Auxiliary calculations for the GK-conductivities in Phython

```
>>> 1./(3*32.7e-8**3*1.380658e-23*300)*1e-8**2*1.60217733e-19**2*0.04888**(-2)*1e12*0.00095902
0.0023714531734467903
>>> 1./(3*32.7e-8**3*1.380658e-23*300)*1e-8**2*1.60217733e-19**2*0.04888**(-2)*1e12*0.0012802
0.0031656632318894087
>>> 1./(3*32.7e-8**3*1.380658e-23*300)*1e-8**2*1.60217733e-19**2*0.04888**(-2)*1e12*0.0012394
0.0030647734803966047
>>> 1./(3*32.7e-8**3*1.380658e-23*300)*1e-8**2*1.60217733e-19**2*0.04888**(-2)*1e12*0.0013079
0.0032341594602313373
```

F.   Auxiliary calculations for the EH-conductivities in Phython

```
>>> 1./(6*32.7e-8**3*1.380658e-23*300)*1.60217733e-19**2*1e-8**2*1e12*1.2313
0.0036373338768437391
>>> 1./(6*32.7e-8**3*1.380658e-23*300)*1.60217733e-19**2*1e-8**2*1e12*0.25653
0.00075780496989094799

>>> 1./(6*38.4e-8**3*1.380658e-23*300)*1.60217733e-19**2*1e-8**2*1e12*0.84077
0.0015337199964118315
>>> 1./(6*38.4e-8**3*1.380658e-23*300)*1.60217733e-19**2*1e-8**2*1e12*0.29647
0.00054081611776849283
```

```
>>> 1./(6*34.1e-8**3*1.380658e-23*300)*1.60217733e-19**2*1e-8**2*1e12*2.5471
0.0066350684085439886
>>> 1./(6*34.1e-8**3*1.380658e-23*300)*1.60217733e-19**2*1e-8**2*1e12*1.5779
0.0041103507682625573
>>> 1./(6*34.1e-8**3*1.380658e-23*300)*1.60217733e-19**2*1e-8**2*1e12*1.0803
0.0028141275967767544

>>> 1./(6*60.13e-8**3*1.380658e-23*400)*1.60217733e-19**2*1e-8**2*1e12*4.0204
0.0014325819079742438
>>> 1./(6*60.13e-8**3*1.380658e-23*400)*1.60217733e-19**2*1e-8**2*1e12*0.89711
0.00031966559433458703
>>> 1./(6*60.13e-8**3*1.380658e-23*400)*1.60217733e-19**2*1e-8**2*1e12*0.84049
0.00029949029147181177

>>> 1./(6*67.0e-8**3*1.380658e-23*300)*1.60217733e-19**2*1e-8**2*1e12*3.1178
0.0010707458272543032
>>> 1./(6*67.0e-8**3*1.380658e-23*300)*1.60217733e-19**2*1e-8**2*1e12*4.7031
0.0016151852909614833

>>> 1./(6*65.2e-8**3*1.380658e-23*300)*1.60217733e-19**2*1e-8**2*1e12*17.887
0.0066658765406850682
>>> 1./(6*65.2e-8**3*1.380658e-23*300)*1.60217733e-19**2*1e-8**2*1e12*9.6426
0.0035934690630742908
>>> 1./(6*65.2e-8**3*1.380658e-23*300)*1.60217733e-19**2*1e-8**2*1e12*14.423
0.0053749615556717579

>>> 1./(6*65.2e-8**3*1.380658e-23*300)*1.60217733e-19**2*1e-8**2*1e12*10.356
0.0038593289794451031
```

[1] P. Wasserscheid and W. Keim, Angew. Chem. **39**, 3772 (2000).

[2] A. Oleinikova, P. Sasusanker, and H. Weingärtner, J. Phys. Chem. B **108**, 8467 (2004).

[3] F. Kremer and A. Schönhals, *Broadband Dielectric Spectroscopy* (Springer, Berlin, 2002).

[4] J. P. Hansen and I. R. MacDonald, *Theory of Simple Liquids* (Pergamon, New York, 1986), 2nd ed.

[5] A. R. Leach, *Molecular Modelling: Principles and Applications* (Pearson Education, 2001).

[6] M. P. Allen and D. J. Tildesley, *Computer simulations of liquids* (Oxford Press, New York, 1989).

[7] D. Frenkel and B. Smit, *Understanding Molecular Simulation: From Algorithms to Applications* (Academic Press, 2002).

[8] T. Baştuğ and S. Kuyucak, Chem. Phys. Lett. **408**, 84 (2005).

[9] D. Evans and G. Morriss, *Statistical Mechanics of Non-Equilibrium Liquids* (http://rsc.anu.edu.au/~evans/evansmorrissbook.php, 1990).

[10] R. Kubo, J. Phys. Soc. Jpn. **12**, 570 (1957).

[11] J. Honerkamp and H. Römer, *Klassische Theoretische Physik* (http://www.freidok.uni-freiburg.de/volltexte/82/, 1993).

[12] C. J. F. Böttcher and P. Bordewijk, *Theory of electric polarization*, vol. 2 (Elsevier, Amsterdam, 1978).

[13] C. Schröder, C. Wakai, H. Weingärtner, and O. Steinhauser, J. Chem. Phys. **126**, 084511 (2007).

[14] B. J. Berne and R. Pecora, *Dynamic light scattering* (Dover Publications, Mineola, New York, 2000).

[15] B. R. Brooks, R. E. Bruccoleri, B. D. Olafson, D. J. States, and S. Swaminathan, J. Comput. Chem. **4**, 187 (1983).

[16] A. D. MacKerell, B. Brooks, C. L. Brooks, L. Nilson, B. Roux, Y. Won, and M. Karplus, *The Encyclopedia of Computational Chemistry*, vol. 1 (John Wiley, 1998).

[17] C. Schröder, T. Rudas, and O. Steinhauser, J. Chem. Phys. **125**, 244506 (2006).

[18] C. Schröder, T. Rudas, G. Neumayr, W. Gansterer, and O. Steinhauser, J. Chem. Phys. **127**, 044505 (2007).

[19] C. Schröder, M. Haberler, and O. Steinhauser, J. Chem. Phys. **???**, ??? (2008).

[20] J. N. C. Lopes, J. Deschamps, and A. A. H. Padua, J. Phys. Chem. B **108**, 2038 (2004).

[21] C. G. Hanke, S. L. Price, and R. M. Lynden-Bell, Mol. Phys. **99**, 801 (2001).

[22] C. Rey-Castro and L. F. Vega, J. Phys. Chem. B **110**, 14426 (2006).

[23] J. Pićalek and J. Kolafa, J. Mol. Liquids **134**, 29 (2007).

[24] H. Tokuda, K. Hayamizu, K. Ishii, A. B. H. Susan, and M. Watanabe, J. Phys. Chem. B **108**, 16593 (2004).

[25] C. Cadena, Q. Zhao, R. Q. Snurr, and E. J. Maginn, J. Phys. Chem. B **110**, 2821 (2006).

[26] T. I. Morrow and E. J. Maginn, J. Phys. Chem. B **106**, 12807 (2002).

[27] C. J. Margulis, H. A. Stern, and B. J. Berne, J. Phys. Chem. B **106**, 12017 (2002).

[28] Y. T. Tetsuo Nishida and M. Yamamoto, Journal of Fluorine Chemistry **120**, 135 (2003).

[29] E. I. Cooper and E. J. M. Sullivan, in *Proc. 8th Int. Symp. Molten Salts*, edited by P. N. The Electrochem. Soc. (1992), pp. 386–396.

[30] H. Tokuda, S. Tsuzuki, A. B. H. Susan, K. Hayamizu, and M. Watanabe, J. Phys. Chem. B **110**, 19593 (2006).

[31] J. A. Widegren, A. Laesecke, and J. W. Magee, Chem. Commun. pp. 1610–1612 (2005).

[32] P. Bonhôte, A.-P. Dias, N. Papageorgiou, K. Kalyanasundaram, and M. Grätzel, Inorg. Chem. **35**, 1168 (1996).

[33] Y. Yoshida, O. Baba, and G. Saito, J. Phys. Chem. B **111**, 4742 (2007).

Selected results from this diploma thesis are an integral part of the recent paper "On the computation and contribution of conductivity in molecular ionic liquids", S.Schröder, M.Haberler and O.Steinhauser, J.Chem.Phys. 128 in press, to appear on March 14, 2008.

CURRICULUM VITAE

Michael Haberler

Wien, am 14.03.2008

05.07.1983	geboren in Wien
Sep. 1989 – Jun. 1993	Volksschule in Wien
Sep. 1993 – Jun. 2001	Gymnasium Theresianische Akademie in Wien
Sep. 2001 – Mai 2002	Grundwehrdienst
ab Sep. 2002	Studium Molekulare Biologie an der Universität Wien
Okt. 2005 – Jun. 2006	Erasmus-Stipendium für Aufenthalt an der University of Leicester in Groß Britannien
ab Mär. 2007	Diplomarbeit bei Prof. O. Steinhauser am Institut für Computer-gestüzte biologische Chemie